Geophysical Journal International

Geophys. J. Int. (2018) **0,** 1–0
GJI Geodynamics and tectonics

doi: 10.1093/gji/ggy230

On the interaction of the North Andes plate with the Caribbean and South American plates in northwestern South America from GPS geodesy and seismic data

Omar J. Pérez,[1] Steven G. Wesnousky,[2] Roberto De La Rosa,[1] Julio Márquez,[1] Redescal Uzcátegui,[1] Christian Quintero,[1] Luis Liberal,[3] Héctor Mora-Páez[4] and Walter Szeliga[5]

[1]*Department of Earth Sciences, Simón Bolívar University, Caracas 1080A, Venezuela. E-mail: ojperez@usb.ve*
[2]*Center for Neotectonic Studies, University of Nevada, Reno, NV 89557, USA*
[3]*Department of Geodesy, Central University of Venezuela, Caracas 1050, Venezuela*
[4]*Sptial Geodetic Research Group, Colombian Geological Survey, Bogota 111321, Colombia*
[5]*Department of Geological Sciences, Central Washington University, Ellensburg, WA 98926, USA*

Accepted 2018 June 8. Received 2018 March 27; in original form 2017 April 12

SUMMARY

We examine the hypocentral distribution of seismicity and a series of geodetic velocity vectors obtained from Global Positioning System observations between 1994 and 2015 both off-shore and mainland northwestern South America (66°W–77°W; 8°N–14°N). Our analysis, that includes a kinematic block modelling, shows that east of the Caribbean–South American–North Andes plates′ triple junction at ∼68°W; 10.7°N, right-lateral easterly oriented shear motion (∼19.6 ± 2.0 mm yr^{-1}) between the Caribbean and South America plates is split along two easterly striking, right-lateral strike-slip subparallel fault zones: the San Sebastián fault that runs off-shore the Venezuelan coast and slips about 17.0 ± 0.5 mm yr^{-1} and the La Victoria fault, located on-shore to the south, which is accumulating strain equivalent to 2.6 ± 0.4 mm yr^{-1}. West of the triple junction, relative right-lateral motion between the Caribbean and South American plates is mostly divided between the Morrocoy and Boconó fault systems that strike northwest and southwest from the triple junction, respectively, and bound the intervening North Andes plate that shows an easterly oriented geodetic slip of 15.0 ± 1.0 mm yr^{-1} relative to the South American plate. Slip on the Morrocoy fault is right-lateral and transtensional. Motion across the Boconó fault is also right-lateral but instead transpressional, divided between ∼9 and 11 mm yr^{-1} of right-slip on the Boconó fault and 2–5 mm yr^{-1} of convergence across adjacent and subparallel thrust faults. Farther west of the triple junction, ∼800 km away in northern Colombia, the Caribbean plate subducts to the southeast beneath the North Andes plate at a geodetically estimated rate of ∼5–7 mm yr^{-1}.

Key words: Plate motions; Space geodetic surveys; Earthquake hazards; Seismicity and tectonics; Dynamics: seismotectonics; Kinematics of crustal and mantle deformation.

INTRODUCTION

The purpose of this paper is to combine Global Positioning System (GPS) geodesy-derived velocity vectors and seismological data to assess the kinematics of the relative motion between the Caribbean, South American and North Andes plates in the northwestern tip of South America (Fig. 1), a highly populated region that includes the Venezuelan capital city of Caracas and other major towns in Colombia, including a population of ∼16 million people (INE 2011; DANE 2016).

GPS geodetic investigations have shown that the Caribbean plate slips easterly at a rate of ∼19.6 ± 2 mm yr^{-1}(Pérez *et al.* 2001; Weber *et al.* 2001) relative to the South American plate. Understanding of how this motion is distributed is complicated by the presence of the Caribbean–North Andean–South American triple junction (Fig. 1) proposed by Pérez *et al.* 1997a, Pérez & Mendoza 1998 and Bird 2003, and for this reason has remained somewhat elusive. This type of junction formed by three strike-slip faults is unstable and it is required that the faults have the same sense of relative motion (McKenzie & Morgan 1969). To the west of the triple junction, complexity arises because relative motion between

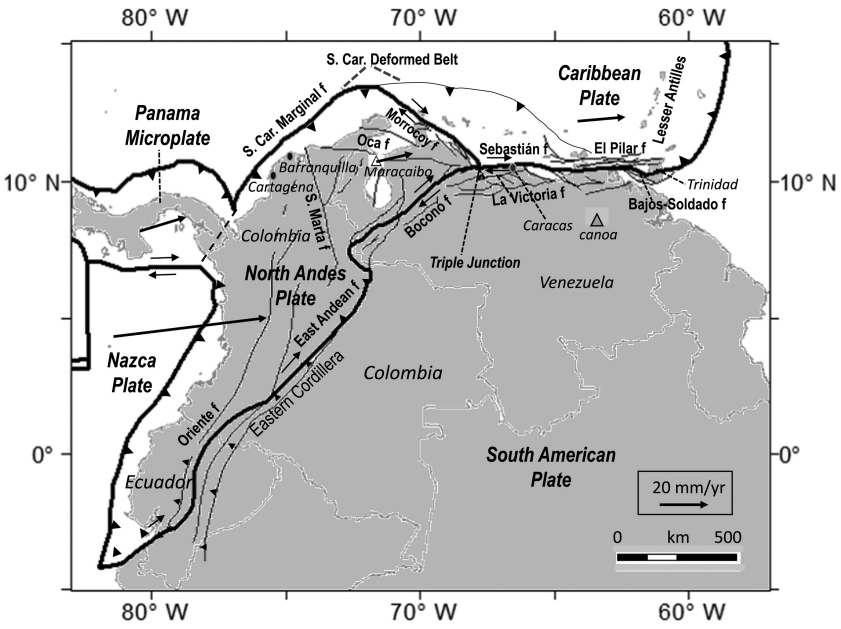

Figure 1. Tectonic setting of the southern Caribbean and adjacent plates (compiled from Silver *et al.* 1975; Pérez & Aggarwal 1981; Kellogg & Vega 1995; Pérez *et al.* 1997b; Trenkamp *et al.* 2002; Bird 2003; Gorney *et al.* 2007; Magnani *et al.* 2009; Weber *et al.* 2009; Camacho *et al.* 2010; Escalona & Mann 2011; Kroehler *et al.* 2011). Main plate boundaries are shown by thick lines. Oceanic segments with teeth indicate subduction with teeth on overthrust plate. The North Andes plate (Trenkamp *et al.* 2002; Bird 2003) is addressed as a block by several authors (Pennington 1981; 1995; Kellogg *et al.* 1985). Plate motions (arrows) are relative to stable South America (DeMets *et al.* 1990; Pérez *et al.* 2001; Weber *et al.* 2001; Trenkamp *et al.* 2002; Pérez *et al.* 2011).

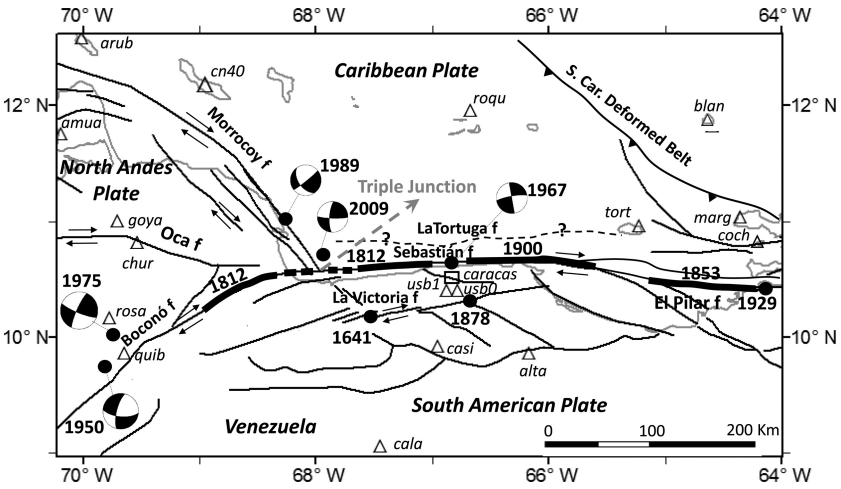

Figure 2. Historical large (M_w 7+) earthquake ruptures (thick lines) in north–central Venezuela since AD 1640. Numerals indicate year of occurrence. Black dots are events of M_w 6+. Triangles are GPS sites visited at various epochs since 1994. f, fault. Focal mechanisms (lower hemisphere, equal area projection) are for events with M_w 6+ since 1950 (Rial 1978; Pérez *et al.* 1997a; Choy 2001; Global CMT Catalog). They show the dextral dominant nature of the Boconó, Morrocoy and San Sebastián faults.

the Caribbean and South American plates is separated by the North Andes plate and divided, as we will show in this paper, between the major northwest striking Morrocoy and southwest striking Boconó fault systems, respectively (Fig. 1; Pérez *et al.* 1997a; Pérez & Mendoza 1998; Bird 2003), with some motion possibly taken up by other faults such as the Oca and Santa Marta faults (Symithe *et al.* 2015). Only along the San Sebastián–El Pilar fault system does motion occur directly between the Caribbean and South American plates. Yet even here, the fault system accommodating the motion and the GPS velocity field reflecting that motion is distributed across an 80–120 km wide zone (Pérez *et al.* 2001; Jouanne *et al.* 2011; Reinoza *et al.* 2015), including other faults such as the La Victoria fault.

A number of large earthquakes have occurred on the main branches of the triple junction since 1640 (Fig. 2). These include a sequence of two events in 1812 (M_w 7.4 and 7.1) that took place within about 1 hr and broke across the triple junction to rupture portions of both the Boconó and San Sebastián faults (Fielder 1961; Altez 1998; Choy *et al.* 2010). In 1900, an M_w 7.6 shock (Pacheco & Sykes 1992) broke the eastern segment of the San Sebastián fault, as recognized from both intensity observations (Centeno-Graü 1900; Sievers 1905; Choy *et al.* 2010) and marine geophysics studies (Colón *et al.* 2015). A number of moderate (M_w ~6+) yet destructive dextral strike-slip shocks are documented (Fig. 2) along the Boconó fault in 1950 and 1975, as well as the San Sebastián fault

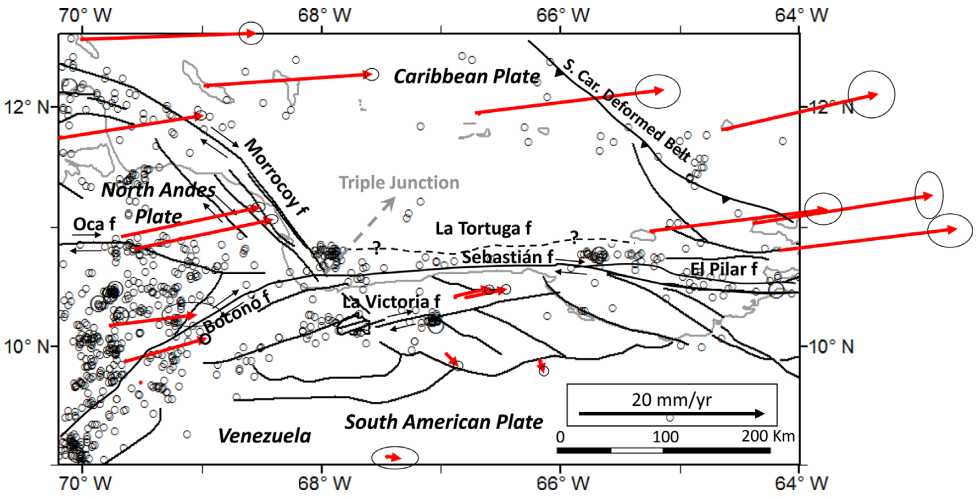

Figure 3. Epicentral locations (circles) of seismicity ($M_w \geq 2.5$) reported by the Venezuelan National Seismological Array (FUNVISIS 2016) in north–central Venezuela and south–central Caribbean from 2003 to 2012. Small-sized circles are microearthquakes of $M_w < 4.5$. Red arrows are GPS velocity vectors relative to South America either compiled or derived in this study. Ellipses are 2-D errors, $\pm 1\sigma$.

in 1967 and 2009, the Morrocoy fault in 1989 (M_w 6.2) and the La Victoria fault in 1641 and 1878 (Pérez *et al.* 1997b). The damaging effects of the latter events are described in detail by Centeno-Graű (1940), Grases (1980) and Ernst (1878). Focal mechanisms of small earthquakes along La Victoria fault also show dextral motion along strike (Pérez *et al.* 1997b). Microseismicity ($M_w < 4$) has been reported on each of the major branches of the triple junction (Fig. 3; e.g. Pérez *et al.* 1997b; Pérez & Mendoza 1998). No significant earthquake activity is reported along La Tortuga fault (Fig. 2) or along the Oca and Santa Marta faults (Fig. 1) since the colony times. The known seismicity record along the Caribbean subduction in northern Colombia (Fig. 1) is limited to a small quantity of teleseismically located events and microseismicity recorded since 1993.

To check and quantify the style and sense of motion of the various active faults that define the branches of the triple junction and ultimately better define the tectonics of northwestern South America, we here conduct an integrated analysis of a series of new GPS observations collected in north–central and northwestern Venezuela and Colombia during the period from 1999 to 2015 and seismological data, including well located sets of microearthquakes reported by the Colombian (1993–2011) and Venezuelan (2003–2012) broad-band national seismological arrays operated by the Colombian Geological Survey (Colombian Geological Survey 2016) and the Venezuelan Foundation for Seismological Research (FUNVISIS 2016), respectively.

In the next sections, we describe the GPS data acquisition and analysis methods and the velocity vectors and field subsequently obtained. Next, we present details of the models that were used to emulate the velocity field across the San Sebastián and La Victoria faults in north–central Venezuela. Then, we analyse the seismicity and the velocity field observed in western Venezuela, which encompasses the Bocono and Morrocoy faults and northern Colombia where the Caribbean plate is being subducted to the south–east beneath the North Andes plate (Fig. 1) along the South Caribbean Marginal fault (Toto & Kellogg 1992; Pérez *et al.* 1997b; Trenkamp *et al.* 2002). Then, we performed a kinematic block modelling for the southern Caribbean plate boundary to further analyse and quantify the regional GPS velocity field and rate and sense of motion along the major active faults that mark the plate boundary. For the analysis we used the modelling approach and associated software 'Blocks' of Meade & Loveless (2009). Finally, the implications of the geodetic findings for regional tectonics and for the quantification of seismic hazards in the region are discussed.

GPS METHODS AND ANALYSIS

GPS data in Venezuela and adjacent regions were obtained using dual frequency receivers during a series of 5–15 d and 12–24 hr surveying sessions between 1994 and March 2015. During this whole period the monument CANOA, located deep within stable South America and Maracaibo (MARA; Fig. 1), as well as USB0 and USB1 (replacing USB0 in 2006; Fig. 2) were occupied 7, 10, 7 and 7 times, respectively since 1999, sites CASI and ALTA in 1999, 2000 and 2012; CHUR and AMUA in 1994, 1999 and 2014; ROQU and CALA in 1994, 1999 and 2000; ARUB in 1999 and 2012; ROSA and MONA in 2000 and 2014. We also used data collected since 2012 at sites CN38 and CN40, which belong to the COCOnet permanent GPS array as well as data collected in 1994 and 1999 by Pérez *et al.* (2001) and Pérez *et al.* (2011) to re-calculate several geodetic vectors reported in those papers using newly acquired data in 2014 at those sites.

In general all Venezuelan sites were occupied simultaneously with CANOA, MARA (Fig. 1) and USB0 (or USB1, Fig. 2) or all of them. We used 15 or 30 s sampling intervals and an elevation mask of 15°. Site's positions for each epoch were obtained using simultaneous observations at 8–11 permanent GPS stations of the International GNSS Service located in the Americas and the Caribbean and/or directly relative to CANOA as a fixed reference point to check for consistency. We used the Bernese GPS v. 5.0 (Dach *et al.* 2007) software package to process the data, following the procedures described by these and other authors (e.g. Jouanne *et al.* 2011; Reinoza *et al.* 2015). Additionally, the Space Geodesy Research Group that runs the GeoRED Project in Colombia (Mora-Páez *et al.* 2016a,b) provided us with the velocity vectors they obtained for six GPS sites in Colombia territory that they processed using the GIPSY-OASIS II software v. 6.3. The corresponding velocity vectors at all sites used in this study, calculated in ITRF2008 Epoch 2010 (Altamimi *et al.* 2011), are given numerically in Table 1. The velocities were then calculated in the South America reference frame using the pole

Table 1. Velocities in the ITRF2008 reference frame showing east and north components with one sigma error.

Site ID	Long (°E)	Lat (°N)	V_e (mm yr^{-1})	σ_e (mm yr^{-1})	V_n (mm yr^{-1})	σ_n (mm yr^{-1})	Ref
ALPA	−72.918	11.528	8.7	2.8	13.7	0.9	1
ALTA	−66.178	9.866	−5.1	0.5	9.2	0.5	2
AMUA	−70.188	11.753	9.7	0.6	12.7	0.5	3
ARAY	−63.711	10.655	5.9	2.5	12.9	2.3	4
ARUB	−70.013	12.574	13.0	1.3	11.1	1.2	2
AVES	−63.618	15.667	14.6	2.7	14.9	1.8	4
BAPA	−74.660	5.470	2.8	0.4	14.6	0.7	5
BARB	−59.620	13.250	12.9	1.8	14.3	1.6	4
BARI	−70.381	8.657	−4.9	0.4	12.0	0.3	6
BARU	−75.590	10.258	11.4	0.8	10.3	0.5	1
BATE	−71.110	9.170	1.9	0.4	15.0	0.3	6
BLAN	−64.599	11.822	10.7	2.5	15.0	1.8	4
BUCM	−73.182	7.117	3.0	2.3	13.5	0.8	1, 7
CALA	−67.449	9.061	−3.7	2.5	10.5	1.2	8
CANO	−63.861	8.568	−5.6	0.9	11.5	0.6	2, 8
CAPI	−72.430	5.350	−3.0	0.5	11.5	0.6	5
CART	−75.500	10.360	12.2	0.9	10.5	0.9	1, 7
CARU	−63.244	10.675	7.4	3.1	12.0	2.5	4
CASI	−66.960	9.926	−4.2	0.5	12.0	0.5	2
CHUR	−69.541	10.818	9.4	0.7	13.9	0.5	8
CN35	−81.363	13.374	17.3	−2.7	0.7	0.6	1
CN37	−75.263	10.793	9.0	1.7	13.6	2.1	1
CN38	−71.988	12.222	11.5	0.6	14.1	0.4	1
CN40	−68.960	12.180	12.5	0.7	11.8	0.7	8
COCH	−63.994	10.782	13.2	2	12.6	2	4
DALI	−72.314	8.267	4.4	0.6	11.5	0.5	6
FABI	−61.658	10.098	−1.9	1.2	12.6	1.1	4
FRAI	−70.799	8.850	−1.4	0.4	13.4	0.3	6
FUND	−71.863	7.783	−1.0	0.6	10.3	0.5	6
GOYA	−69.708	10.995	9.1	0.7	13.7	0.5	3
GREO	−61.640	12.220	13.4	0.5	15.0	0.5	8
GRIT	−71.998	8.156	0.3	0.3	10.9	0.2	6
GUAC	−71.333	7.515	−4.6	0.3	10.4	0.3	6
GUAY	−72.342	8.530	6.7	0.6	11.4	0.5	6
JUAN	−63.369	10.357	−3.1	3	12.0	2.6	4
LUCI	−60.970	14.090	12.2	1.8	14.1	1.6	4
MARA	−71.624	10.674	8.8	0.8	12.8	0.8	2
MARG	−64.36	11.042	13.8	1.5	13.7	2.5	4
MONA	−70.460	9.550	−1.0	0.6	12.6	0.5	2
MONT	−75.681	8.895	11.3	0.6	11.1	0.4	1, 7
MZAL	−75.470	5.030	12.3	0.6	17.9	0.4	1, 7
PREG	−71.775	8.029	−1.4	0.3	10.9	0.3	6
QUIB	−69.783	9.914	3.3	3.2	11.9	1.3	3
RION	−75.430	6.176	5.1	0.3	14.7	0.2	1, 7
ROSA	−69.774	10.166	3.1	0.5	13.0	0.5	2
RQUE	−66.678	11.953	14.0	2.4	13.4	1.8	3
STOD	−70.630	8.860	−2.9	0.4	12.7	0.3	3
SANA	−81.720	12.580	12.3	0.4	7.0	0.4	1, 7
TORO	−71.126	9.064	−1.2	0.4	10.5	0.3	3
TORT	−65.227	10.963	13.3	2	13.3	1.7	3
TRIN	−61.400	10.680	12.4	1.4	13.4	1.2	9
USB0	−66.792	10.409	−1.1	0.5	12.0	0.5	2
USB1	−66.883	10.411	−1.4	0.5	12.1	0.5	2
UWAS	−72.390	6.450	0.3	0.4	13.0	0.6	5
VBUV	−73.860	5.530	3.9	0.5	15.6	0.7	5
VDPR	−73.248	10.436	8.5	0.4	15.3	0.4	1
VPOL	−74.861	10.794	7.7	0.8	16.6	0.5	1

1: Mora-Páez *et al.* (2016a); 2: this study; 3: Re-evaluated from Pérez *et al.* (2001); 4: Pérez *et al.* (2001); 5: Mora-Páez *et al.* (2016b); 6: Re-evaluated from Pérez *et al.* (2011); Trenkamp *et al.* (2002); 8: D. Mencin, unpublished data, 2015; 9: Estimated from Weber *et al.* (2001).

of rotation between ITRF2008 and South America provided by Altamimi *et al.* (2012). They are graphically shown in Figs 3, 4 and 8. Finally, we incorporated seven velocity vectors in the Colombian region expressed in the South America reference frame, originally provided by Trenkamp *et al.* (2002), which were re-calculated in the ITRF2008 frame (Mora-Páez *et al.* 2016a).

Table 2. Euler pole locations and rotation rates relative to the South American plate for the best fitting models described in the text.

Block/plate	Latitude (°)	Longitude (°)	Rotation rate (deg Myr^{-1})
(∗) Caribbean	61.9° ± 2.0°	284.3° ± 2.0°	0.229 ± 0.015
Model 4			
Block A	25.2° ± 9.3°	280.7° ± 2.3°	0.575 ± 0.296
Block B	5.1° ± 5.5°	112.2° ± 1.3°	0.403 ± 0.135
Block C	−6.3° ± 6.6°	114.4° ± 2.1°	0.339 ± 0.499
Model 5			
Block A	22.0° ± 6.2°	281.3° ± 1.6°	0.672 ± 0.293
Block B	−2.3° ± 1.0°	110.6° ± 0.2°	0.660 ± 0.080
Block C	13.0° ± 2.0°	294.7° ± 1.5°	0.657 ± 0.541
Block D	0.3° ± 1.4°	110.6° ± 0.2°	0.603 ± 0.079
Block E	21.3° ± 35.7°	115.4° ± 5.0°	0.341 ± 0.322

(∗) From Pérez *et al.* 2001.

RESULTS

Slip-partitioning associated with the San Sebastián and La Victoria fault zones

In this section, we combine GPS data with simple elastic strain accumulation models and seismic evidence to constrain slip rate estimates along these two major dextral, easterly striking fault zones. The two faults (Fig. 3) form the Caribbean–South American main plate boundary east of ∼68°W. Our goal is to quantify how the ∼19.6 mm yr^{-1} in the N85°E direction of Caribbean–South American rate of relative motion, indicated by the corresponding pole of rotation (Table 2) derived from GPS geodesy (Pérez *et al.* 2001), is distributed between these fault zones. N85°E is also the strike direction of the San Sebastián fault.

Fig. 3 shows the seismicity (moment magnitude $M_w \geq 2.6$, circles) reported by FUNVISIS (2016) for the period 2003–2012 together with the GPS-derived velocity vectors (arrows) relative to stable South America, in north–central Venezuela. About 98.5 per cent of the seismic events reported are microearthquakes in the M_w range of 2.6–4.4. Only minor activity is observed in the inner regions of the Caribbean, though a series of seismological stations are located in Venezuelan islands and along the northern coast of the country (see http://www.funvisis.gob.ve/). FUNVISIS catalog shows a fairly constant rate of listing for events with $M_w \geq 2.6$ during the time span under consideration.

East of ∼68°W the San Sebastián and La Victoria faults coexist. These fault zones are nearly parallel (Fig. 3), making an angle of ∼5°–10° and are separated by a distance that ranges from ∼30–50 km. Recent marine geophysics studies show that at some places the San Sebastián fault is multibranched and the fault zone reaches a width of 10–12 km (Colón *et al.* 2015). As found out by Pérez *et al.* (1997b) from a different set of earlier earthquakes, most of the seismic activity in the region straddles both fault zones, occurs in general at focal depths shallower than ∼14 km and focal mechanisms commonly show dextral motion on easterly oriented vertical fault planes (Figs 2 and 4). These observations show that these two fault zones accommodate most of the relative motion between the Caribbean and South American plates in the region.

Fig. 5 is a stacked profile showing the N85°E velocity component of GPS sites located to the north and south of the San Sebastián and La Victoria faults. The stations used in the stack are marked in Fig. 4 with blue stars. Many benchmarks were vandalized since the first occupations in 1999 and thus the number of data points remains relatively few. Nonetheless, the velocities of USB0 and USB1 are very well constrained since all together they have been occupied 14 times since 1999 and their location between the two faults provides strong constraints on the slip partitioning we next describe.

The field (Fig. 5) across these faults is confined to a shear zone <120 km wide and most of the surface deformation is contained within a 70–80 km wide zone encompassing the San Sebastián and La Victoria faults. The dashed line in Fig. 5 is the elastic modelled surface velocities (Okada 1985; Dixon *et al.* 1998) for a single, N85°E oriented vertical fault taken up the full Caribbean–South American relative motion (∼19.6 mm yr^{-1}). The solid line is in contrast calculated for a system of two subparallel vertical faults (i.e. The La Victoria and San Sebastián faults) separated by a distance of 45 km, in both cases with dextral shear below a locking depth of 14 Km. The two-fault model provides a good fit for the observed data, and corresponds to a dextral shear of 2.6 ± 0.4 mm yr^{-1} for La Victoria fault and 17.0 ± 0.5 mm yr^{-1} for San Sebastián fault, below a locking depth of 14 ± 3 km.

The modelling result does not preclude the possibility of some portion of slip modelled on the San Sebastián fault being accommodated on other faults to the north such as the easterly striking La Tortuga fault (Fig. 2). One could, for example, allow up to ∼3 mm yr^{-1} of slip along La Tortuga fault by decreasing a similar amount of modelled slip on the San Sebastián fault, without violating the observations. We hesitate to argue for this latter possibility because both the seismic record and marine geophysics studies (Colón *et al.* 2015) do not support the existence of the La Tortuga fault along the entire north–central coast of Venezuela. Similarly, it is possible that the plate boundary may include a third fault farther north along the easterly striking section of the South Caribbean Deformed Belt in the off-shore area (Fig. 1), with a small and probably negligible amount of slip on that portion of the structure (Symithe *et al.* 2015), expressed by an actively deforming accretionary prism (Gorney *et al.* 2007; Clark *et al.* 2008; Magnani *et al.* 2009; Escalona & Mann 2011; Kroehler *et al.* 2011). Finally, based on GPS investigations there is general agreement (Pérez *et al.* 2001; Clark *et al.* 2008; Jouanne *et al.* 2011; Reinoza *et al.* 2015; Symithe *et al.* 2015) in that east of ∼65.5°W in eastern Venezuela (Figs 1 and 2) the easterly striking El Pilar fault zone is the main strand of the Caribbean–South America plate boundary, taking up most of the relative motion between the two plates. In our interpretation, both the San Sebastián and La Victoria faults merge around 65.5°W with the El Pilar fault zone so that their motion is absorbed into the single El Pilar strand.

The interaction of the North Andes plate with the Caribbean and the South American plates in western Venezuela and northern Colombia

Numerous authors (e.g. Dewey 1972; Pennington 1981; Kellogg & Bonini 1982; Kellogg 1984; Toto & Kellogg 1992; van der Hilst & Mann 1994; Malavé & Suárez 1995; Pérez *et al.* 1997b; Pérez & Mendoza 1998; Trenkamp *et al.* 2002; Pérez *et al.* 2011; Bernal-Olaya *et al.* 2015; Chiarabba *et al.* 2015; Syracuse *et al.* 2016; Mora-Páez *et al.* 2016b) have studied the seismicity and tectonics of northwestern South America. There is a general agreement that along the northwestern tip of the continent there exists a northeast-trending slab of Caribbean plate that is subducting along the South Caribbean Marginal fault to the southeast (Figs 1 and 6) beneath the North Andes plate (Toto & Kellogg 1992; Trenkamp *et al.* 2002; Bird 2003). Here we shall re-visit the seismicity of the region using teleseismic locations ($m_b \geq 4.5$) reported in the revised catalogues

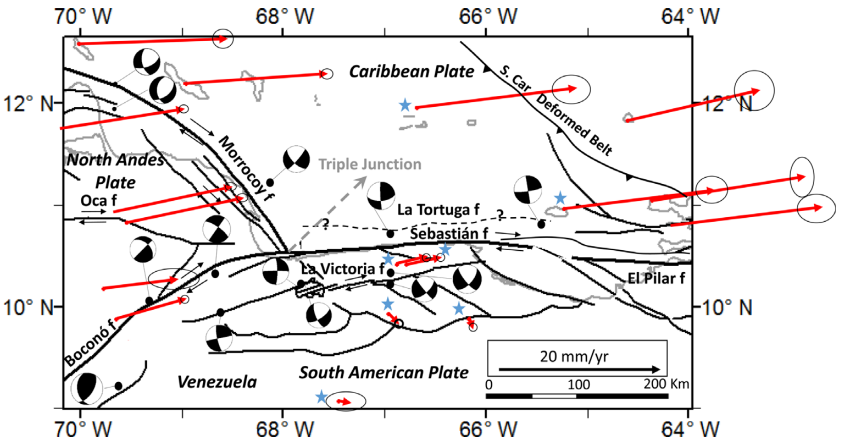

Figure 4. Representative focal mechanisms of microearthquakes reported by several authors in north–central Venezuela (Pérez *et al.* 1997a,b; Audemard *et al.* 2005) and GPS velocity vectors. Focal Mechanisms straddling the Boconó fault show dextral slip and reverse faulting. Those along the Morrocoy fault show a combination of dextral slip and normal faulting. San Sebastián fault shows dextral motion. La Victoria fault shows dextral slip along strike and southeast dextral motion (right-stepping offset) at places where it is intercepted by southeast striking dextral slip faults. GPS vectors marked with a blue star are used to construct Fig. 5.

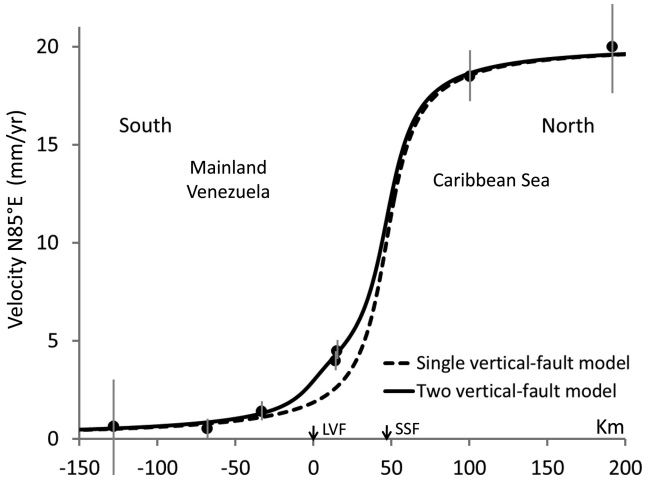

Figure 5. Velocity field in north–central Venezuela and south–central Caribbean. Dots are the N85°E component of the observed velocity vectors at sites marked with a red star in Fig. 4, located to the north and south of the San Sebastián and La Victoria faults, ± 1σ uncertainties (bars). Broken line is the modelled surface velocities due to 20 mm yr^{-1} of dextral shear below a locking depth of 14 km on a single, N85°E trending vertical fault. Solid line is the corresponding modelling for two subparallel faults located 47 km apart, namely La Victoria and San Sebastián faults, with a slip rate of 2.6 and 17 mm yr^{-1}, respectively.

of the ISC for the period 1980–2013, as well as microearthquake locations ($2.5 < m_b < 4.5$) reported in Colombian territory by the Colombian Geological Survey (Colombian Geological Survey 2016) for the period 1993–2015 and by FUNVISIS (2016) for the period 2003–2012 in Venezuelan territory, followed by the analysis of GPS-derived velocity vectors and their tectonic implications.

The epicentral locations are plotted as a function of increasing depth in Fig. 6. The distribution of seismicity defines an inclined northeast striking slab dipping southeasterly in northwestern Venezuela and northern Colombia. The top of the interpreted slab is defined by the series of depth contours (dotted lines) shown in the figure. These contours illustrate the northeast strike and southeast dip of the Benniof zone that defines the subduction of the Caribbean slab along the South Caribbean Marginal fault beneath South America. Three northwest–southeast vertical cross-sections (1–3) are shown and described in Fig. 7 and its caption. Each of them contains the earthquake hypocentres (dots) located within the rectangles 1–3 shown in Fig. 6. The horizontal projection of the dip of the subducted slab as manifest by the seismicity (Fig. 6) is oblique to the calculated slip vector (Pérez *et al.* 2001; Weber *et al.* 2001) of the Caribbean plate relative to South America at 12°N, 77°W (broken arrow in Figs 6 and 8). It is also observed in Fig. 6 that seismicity generally terminates and does not occur northeast of the Morrocoy fault zone, an observation that led Pérez *et al.* (1997b) to conclude that this fault zone marks the northeastern end of the North Andes plate.

Fig. 8 shows a series of GPS velocity vectors (arrows) projected relative to the South American plate reported by several authors (Trenkamp *et al.* 2002; Pérez *et al.* 2011; Mora-Páez *et al.* 2016a,b; this study) at sites within the northernmost regions of the North Andes plate and adjacent Caribbean and South American areas. The GPS vectors at sites located in the northern inner regions of the North Andes plate (marked with blue stars in Fig. 8) show an average magnitude of 15.0 ± 1.0 mm yr^{-1} and are easterly oriented (average Az 80° ± 6°), which for reference is the motion of site MARA. The 19.6 mm yr^{-1} relative motion of the Caribbean plate with respect to the South American plate, shown by a dashed arrow at two places in Fig. 8, is calculated from the corresponding pole of rotation provided by Pérez *et al.* (2001). To shift the reference frame to the North Andes plate we subtract the MARA vector from all other plotted vectors in Fig. 8. The result is shown in Fig. 9 and along with Fig. 8 serves to illustrate the rate and sense of displacements occurring at the boundaries of the North Andes plate.

It is observed with the vectors in Fig. 9 that the Caribbean plate is subducting at rate of ~5–7 mm yr^{-1} beneath the North Andes plate and that motion along each the Morrocoy and Boconó faults boundaries is right-lateral. As well, there is an obliquity of motion along the Boconó and Morrocoy boundaries that predicts each to have a component of transpression and transtension, respectively. Thus, the Morrocoy fault can be interpreted as a continental rift apart boundary, as pointed out by Bird (2003), at the same time being a dextral shear zone that transforms the Caribbean subduction in northwestern South America into pure east–west strike-slip motion

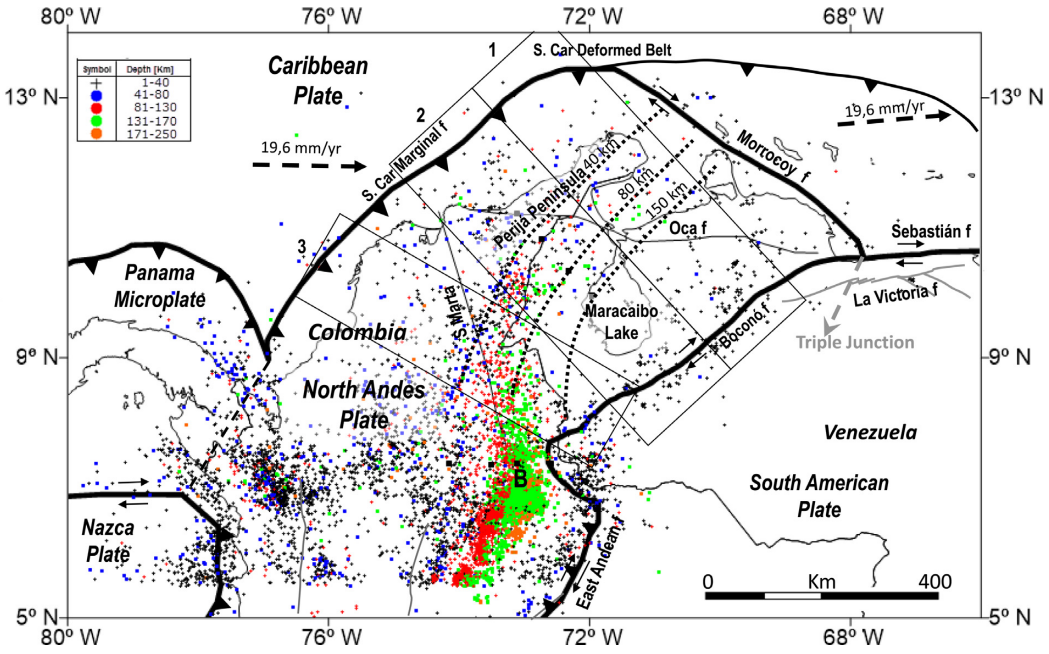

Figure 6. Seismicity in the northwestern tip of South America. Epicentres are discriminated only by their focal depth (h) as indicated in the figure. Catalogues used: ISC (2013) revised for $M_w > 4.5$ from 1980 to 2013; FUNVISIS (2016) from 2003 to 2012 and Colombian Geological Survey (2016) from 1993 to 2011, for $2.5 < M_w < 4.5$. f, fault. Boxes 1–3 comprise the hypocentres that are used to define the Benioff zone and subducted Caribbean slab in those regions, shown in Fig. 7. Broken arrows show calculated slip rate (Pérez *et al.* 2001; Weber *et al.* 2001) of the Caribbean plate relative to South America at those locations. Dotted sinuous lines are depth contours to the top surface of the inclined Caribbean slab, whose southern tip appears to collide at depth with the easterly subducted Nazca slab beneath Bucaramanga (B; Syracuse *et al.* 2016).

along the easterly oriented San Sebastián fault in north–central Venezuela.

Similarly, it is observed in Fig. 9 that South America is moving about 15 mm yr^{-1} at an azimuth of 260° relative to the North Andes plate. Assuming the relative motion is mostly accommodated by deformation along trend of the Boconó fault system, the GPS vectors and model in Fig. 9 indicate about 9–11 mm yr^{-1} of dextral motion and 2–5 mm yr^{-1} of contraction across the fault, consistent with the geodetic results reported by Pérez *et al.* (2011; see their figs 3 and 4) and Symithe *et al.* (2015). The interaction between the North Andes and South American plates along the northeast striking Boconó fault zone in the Venezuelan Andes has been studied using seismic and geomorphological data as well as GPS-derived velocity vectors (e.g. Pérez *et al.* 1997b, 2011; Pérez & Mendoza 1998; Wesnousky *et al.* 2012; Guzmán *et al.* 2013; Symithe *et al.* 2015). Our additional GPS vectors confirm their main results which indicate that due to the obliqueness of the Boconó fault relative to the easterly oriented slip of the North Andean plate relative to South America, this slip is partitioned into 9–11 mm yr^{-1} of dextral motion in the far field of the Boconó fault and a compressive regime perpendicular to the Andes that results in 2–5 mm yr^{-1} of horizontal shortening across the ranges and seismically active thrust faulting along the foothills (Wesnousky *et al.* 2012).

Several faults with slip rates estimated on the order 2 mm yr^{-1} or less occur within the northern tip of the North Andes plate and may also accommodate a small fraction of the Caribbean–South America relative motion (Audemard 1996; Audemard & Audemard 2002; Symithe *et al.* 2015). The Oca and Santa Marta faults (Figs 8 and 9) are the longest and most prominent of these slower slipping faults (Audemard & Audemard 2002; Audemard *et al.* 2005; Symithe *et al.* 2015). These faults have not shown the occurrence of significant earthquake activity since the colony times but palaeoseismicity studies show they have generated earthquakes in recent (Quaternary) times (Audemard 1996; Idárraga-García & Romero 2010). In the next section, we perform a kinematic block motion analysis aimed to better quantify the rate of motion taking place along each of the main active faults of the southern Caribbean plate boundary, with emphasis in our study area, that is, the northwestern tip of South America, including the Morrocoy, Oca and Santa Marta faults.

KINEMATIC BLOCK MODELLING

We use GPS observations in conjunction with the linear block theory and associated code 'Blocks' presented in Meade & Loveless (2009) to estimate slip rates on the major active faults and partitioning of deformation occurring along the southern Caribbean plate. The kinematic block modelling approach is used to study regional GPS velocity fields and quantify the rates of motions along locked or partially locked active faults that form a plate or block boundary (e.g. McCaffrey 2002; Meade *et al.* 2002; Reilinger *et al.* 2006; Loveless & Meade 2010; Saria *et al.* 2014; Symithe *et al.* 2015). It can also be used to confirm or reject a proposed fault boundary.

To perform the modelling we assume for analysis the plate boundary geometry provided by Symithe *et al.* (2015) for the Lesser Antilles, the Trinidad region and northeastern Venezuela (Fig. 10). The geometry is based on their analysis of the seismicity along the Lesser Antilles, the results and interpretations of Weber *et al.* (2009) for the Trinidad and surrounding areas, and Pérez *et al.* (2001) analysis showing the El Pilar fault as the main strand of the Caribbean plate boundary in northeastern Venezuela. West of 65°W the main South American block boundaries faults tested are (Fig. 10) the San Sebastián (S), La Victoria (V), Boconó (B), Oca

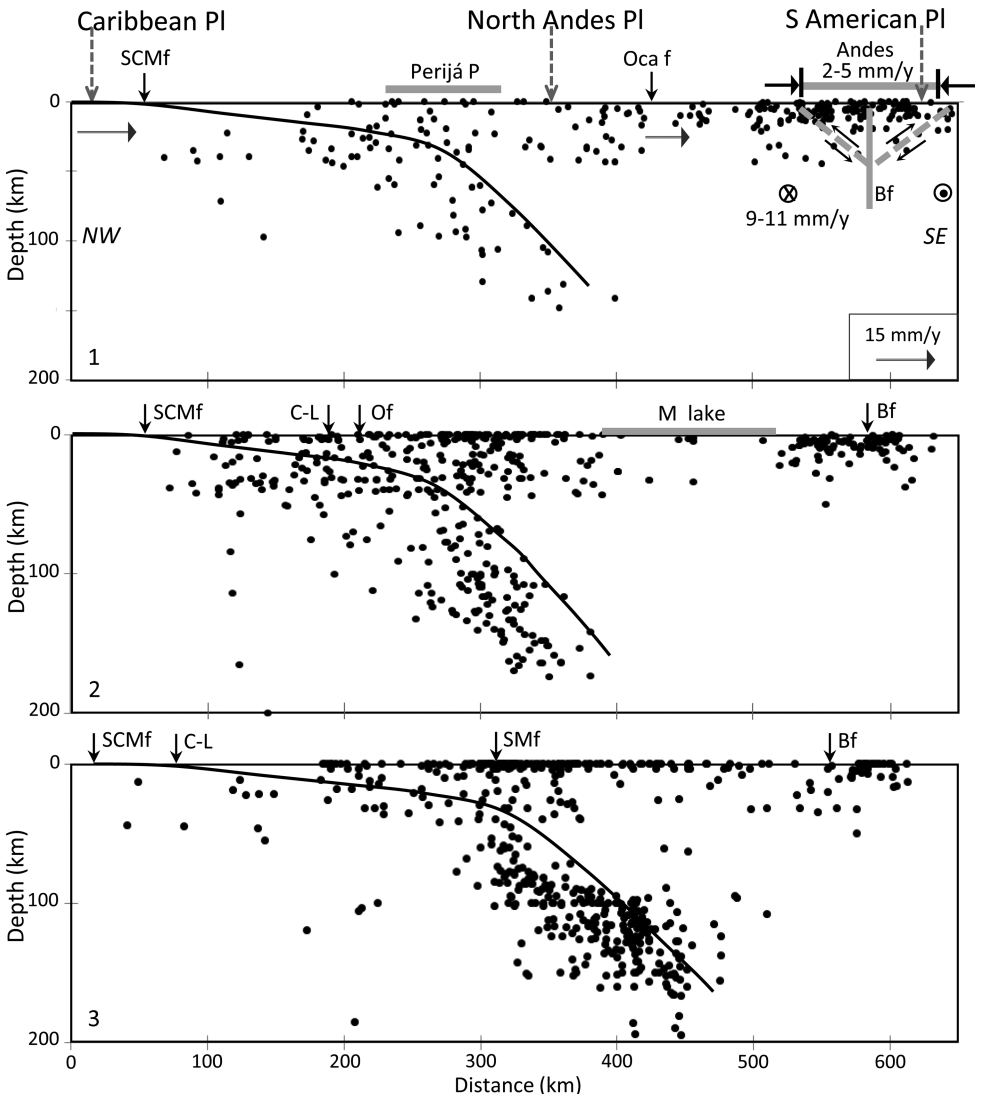

Figure 7. Northwest–southeast vertical cross-sections of earthquake hypocentres whose epicentres are located within the corresponding rectangles 1 in the north to 3 in the south shown in Fig. 6. These cross-sections clearly define the Benioff zone and Caribbean slab subducting to the southeast beneath the North Andes plate in northwestern Venezuela and northern Colombia. Arrows in cross-section 1 show sense of motion relative to South America. Maracaibo (M) Lake and Perijá Peninsula are also shown in Fig. 6 for reference. Faults: SCMf, South Caribbean Marginal; Of, Oca; SMf, Santa Marta; Bf, Boconó. C-L, coast line. In the north (cross-sections 1 and 2) the shallower section of the slab dips ∼10° above a depth of 40 km and 45°–50° below that depth. In the south (cross-section 3) it flattens and the shallower and deeper sections dip ∼5° and ∼35°, respectively. These results were used in our kinematic block motion modelling.

(O), Morrocoy (M), Santa Marta (SM), East Andean (E), South Caribbean Marginal (SCMF) faults and the eastern section of the South Caribbean Deformed Belt (CDB in Fig. 10) east of ∼72°W. This belt has been proposed as an accretionary wedge along which the Venezuelan basin is obliquely subducted beneath South America (Jordan 1975; Silver *et al.* 1975; Talwani *et al.* 1977; Gorney *et al.* 2007; Magnani *et al.* 2009; Escalona & Mann 2011; Kroehler *et al.* 2011). We also examine the effect of the Oca, Morrocoy and Caribbean Deformed Belt faults by assembling and modelling a series of block geometries in which they are systematically included and excluded. In these cases it is assumed, consistent with geology, that the Santa Marta fault must have a left-lateral component of motion (Paris *et al.* 2000; Idárraga-García & Romero 2010), and that motion on the Oca fault must be rather small (<2 mm yr^{-1}), such as indicated by palaeoseismicity studies (Audemard 1996; Audemard *et al.* 2000) and the block motion analysis of Symithe *et al.* (2015).

The set-up of the geometric configuration of the various fault segments used to define each plate or block boundary to be used in all models run was done in the following way: (1) We used a locking depth of 14 km for all strike-slip faults, in agreement with the seismogenic depth reported along the El Pilar, San Sebastián, La Victoria and Boconó faults (all faults are shown in Fig. 1) in seismological studies (e.g. Pérez & Aggarwal 1981; Pérez *et al.* 1997a,b). (2) In the case of a series of subduction segments along the southern Lesser Antilles and Panamá (Fig. 10) we followed Symithe *et al.* (2015) and used a constant dip of 16° and a constant locking depth of 40 km. (3) For the subduction segments along the Southern Caribbean Marginal fault (SCM in Fig. 10) we used a locking depth of 40 km and a dip of 10°, except along its southwest segment where we used 5°, all according to the seismicity profiles shown in Fig. 7. The same locking depth (40 km) and a dip of 13° obtained by Schmitz *et al.* (2008) is used for the east section of the

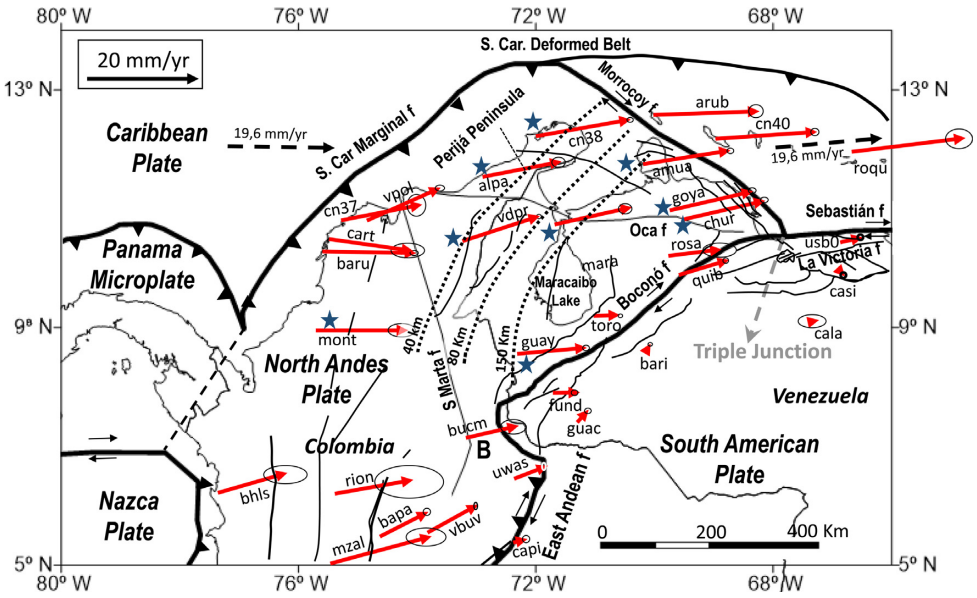

Figure 8. GPS velocity vectors (red arrows) relative to the South American plate in northwestern South America. Ellipses are ± 1σ uncertainties. Blue stars mark the velocity vectors used to estimate the relative slip of the North Andes plate relative to the South American plate in the northwestern tip of South America. B, Bucaramanga.

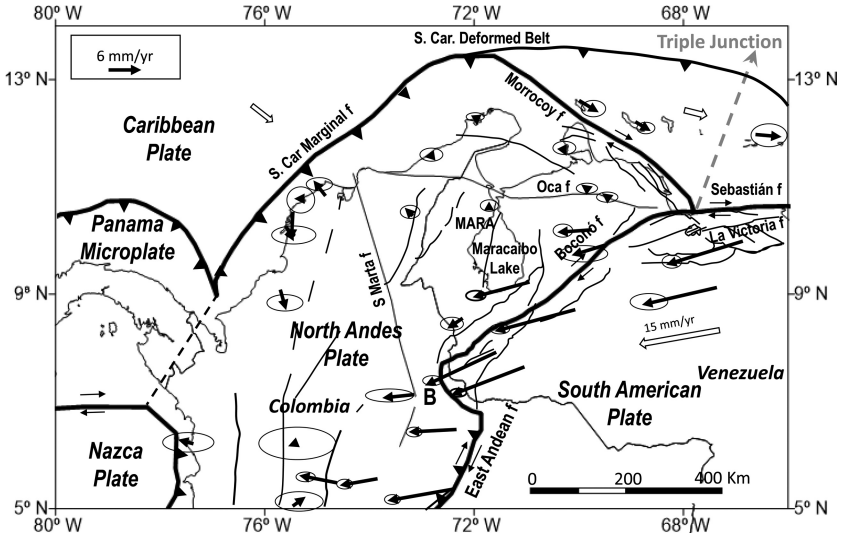

Figure 9. Estimated motion (open arrows) of the Caribbean and South American plates relative to the North Andes plate. Black arrows are the corresponding velocity vectors at each GPS site. Site Mara and other sites in the inner regions of the North Andes plate show little or no motion in the North Andes reference frame. B, Bucaramanga.

South Caribbean Deformed Belt east of 72°W (CDB in Fig. 10). (4) All our analyses are done in the South American (fix) reference frame. Following Manaker *et al.* (2008) we constrain the angular velocity of the Caribbean plate, in our case relative to the South American plate, using the Pérez *et al.* (2001) pole of rotation given in Table 2.

Fig. 10 shows a series of five tested models (Models 1–5). In Models 1–4 we simultaneously solve for block rotation rates; kinematically consistent, fully coupled, fault slip rates; and effective elastic coupling coefficients, whereas in Model 5 we impose and fix a slip rate on two slow slipping faults, namely the Oca fault and the east-striking section of the Caribbean Deformed Belt east of 72°W, as we later describe. We evaluate each model fit by examining the residual (observed-modelled) velocities estimated by the block model analysis while remaining consistent with the previously mentioned geological constraints on the sense and rate of fault slip of the Santa Marta and Oca faults. We follow the style of Loveless & Meade (2010) in presentation of the results in the figure: the estimated fault slip rates predicted from each modelling of block or plate bounding segments are annotated along each segment. Bold black lines indicate the fault traces, and the corresponding labels give strike (top) and fault-normal (bottom) slip rates and uncertainties. Positive signs are for left-lateral and convergent fault motions, and negative signs for dextral slip and tensional faults. Blue and magenta arrows are the observed and residual (observed-modelled) velocities, respectively. Capital letters in the figure provide fault names. The strengths and weaknesses of each model are discussed in the following paragraphs.

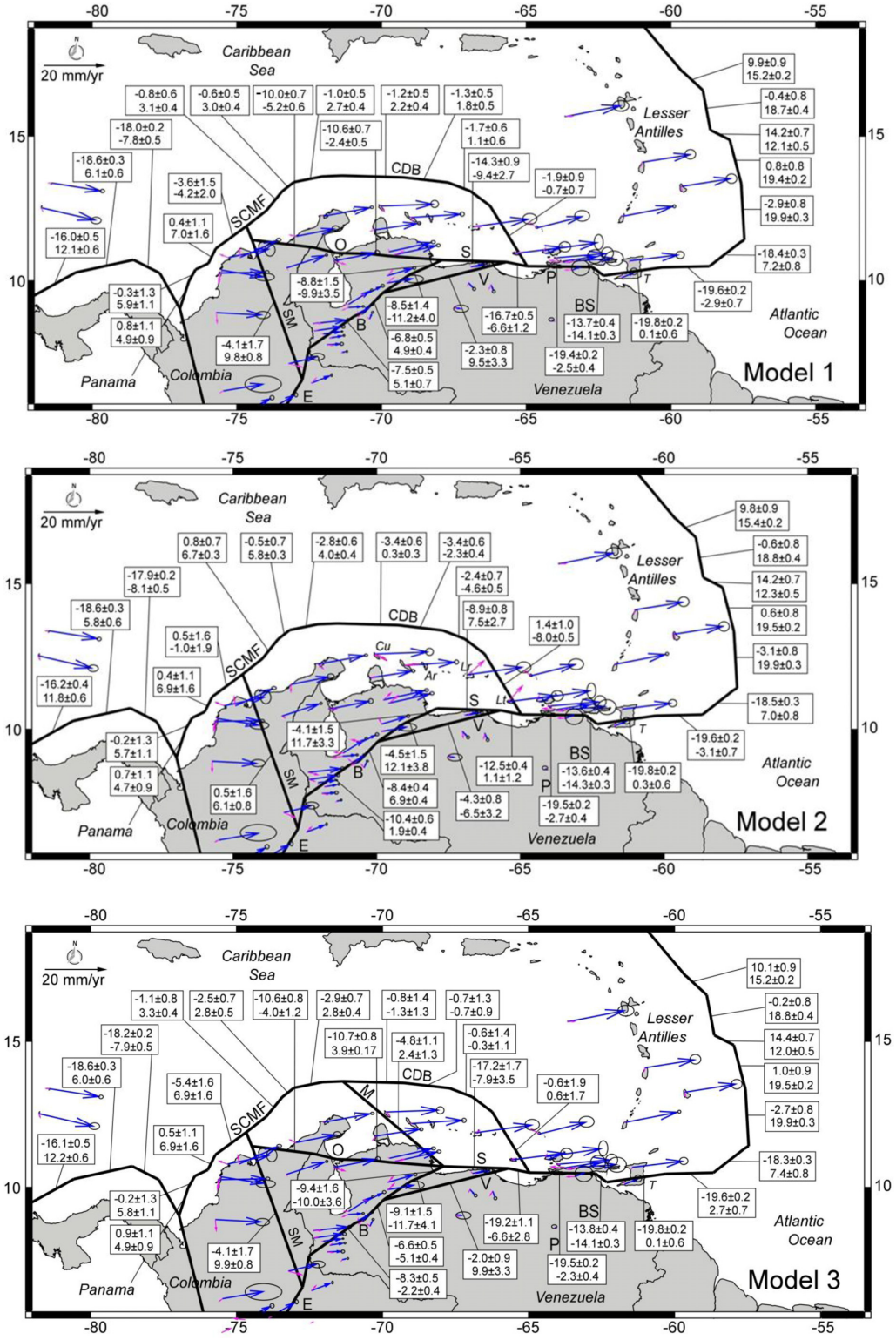

Figure 10. Estimated fault slip rates relative to South America on plate and block bounding segments of southern Caribbean and northern South America for the five models discussed in the text. Bold black lines indicate the fault traces. The corresponding labels give strike (top) and fault-normal (bottom) slip rates and uncertainties. Negative signs indicate dextral and tensile faults; positive signs left-lateral and convergent faults. Blue and magenta arrows are the observed and residual velocity vectors, respectively. Faults: BS, Bajos–El Soldado; P, El Pilar; S, San Sebastián; V, La Victoria; M, Morrocoy; B, Boconó; SM, Santa Marta; E, East Andean; SCMF, South Caribbean Marginal; CDB, South Caribbean Deformed Belt; T, Trinidad. Model 2 provides the names of several islands mentioned in the text: Ar, Aruba; Cu, Curaçao; Lr, Los Roques; Lt, La Tortuga. Models 1–3 are rejected on the basis of geological and geodetic constraints. Model 4 is the block model that best fits the GPS data and geological constraints we used. Model 5 is a hybrid model that incorporates slower slipping faults (O, Oca and CDB, Caribbean Deformed Belt) fixing their slip rates, as explained in the text. Letters within circles in Models 4 and 5 indicate the blocks that configurate each model, whose calculated poles of rotation are given in Table 2.

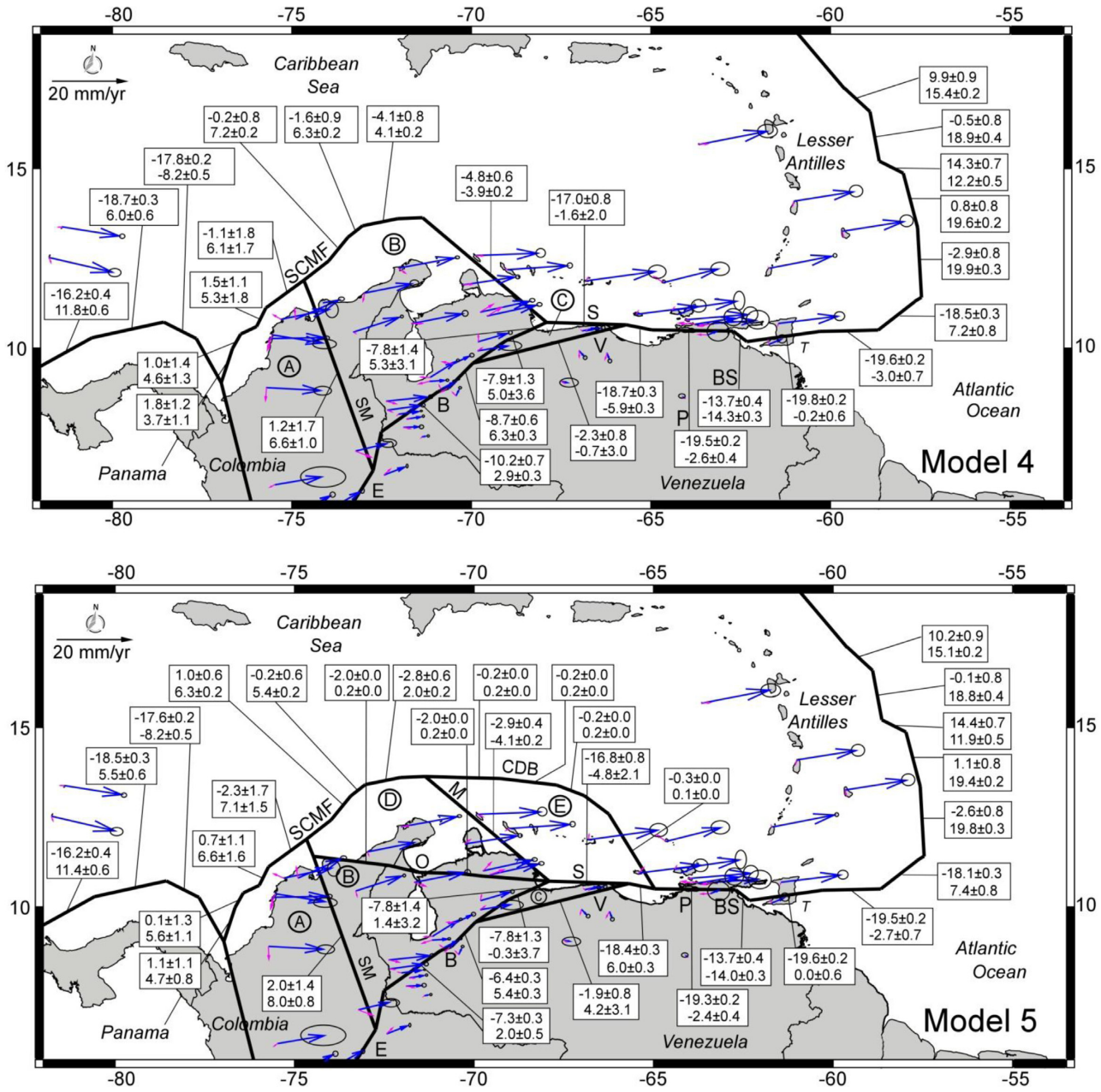

Figure 10. continued.

Model 1 is rejected because the calculated dextral slip rate along the Oca fault (10.0–10.6 mm yr^{-1}) is significantly larger than the slip rate obtained (<2 mm yr^{-1}) from palaeoseismicity studies (Audemard 1996; Audemard *et al.* 2000) and the block motion analysis of Symithe *et al.* (2015). Indeed, changes in direction or magnitude of velocity vectors across the Oca fault (Figs 8 and 9) are within the uncertainties of the data. The large motion modelled for the Oca fault also leads to unacceptably large dextral slip (4.1 mm yr^{-1}) along the Santa Marta fault which is geologically recognized to be a left-lateral fault (Paris *et al.* 2000; Idárraga-García & Romero 2010).

Model 2 is rejected because the combined dextral slip rate modelled along the San Sebastian (S)–La Victoria (V) fault system is only 13.2 mm yr^{-1} and thus it is unable to reproduce the observed velocities (18–20 mm yr^{-1}) on the islands of Aruba (Ar), Curaçao (Cu), Los Roques (Lr) and La Tortuga (Lt), where the residual velocities (magenta arrows in Fig. 10) are very large, in the range of 4–8 mm yr^{-1}. Also, the model shows 3.4 mm yr^{-1} of dextral motion along the east-trending section of the Caribbean Deformed Belt, which clearly violates the observed surface velocity field and subsequent elastic model we derived (Fig. 5) for the north–central Venezuela and south–central Caribbean regions.

Model 3, which includes all faults under consideration, is rejected because as in the case of Model 1, contrary to geology the Santa Marta fault shows a large amount (4.1 mm yr^{-1}) of right-lateral slip and the calculated slip rate along the Oca fault (10.6–10.7 mm yr^{-1}) is significantly higher than the <2 mm yr^{-1} indicated by palaeoseismicity studies (Audemard 1996; Audemard *et al.* 2000; Paris *et al.* 2000; Idárraga-García & Romero 2010).

Models 4 and 5 in Fig. 10 are the two block models that result in velocity fields that best fit the GPS data and geological estimates of fault slip rates. In general, velocity residuals (magenta arrows, Fig. 10) are within measurement uncertainties at most sites. The difference between the two models is the presence in Model 5 of the eastern section of the Caribbean Deformed Belt (CDB in Fig. 10) where we have fixed the total slip at 0.2 mm yr^{-1} (from Symithe *et al.* 2015) along the east-striking section of the belt, and the inclusion of the Oca fault with a fix dextral slip of 2 mm yr^{-1} (Audemard 1996; Audemard *et al.* 2000; Symithe *et al.* 2015). Recall that in Models 1–4 we simultaneously solve for block rotation rates and fault slip rates, whereas in Model 5 we impose and fix a small slip rate on two slow slipping faults, namely the Oca fault and the east-striking section of the Caribbean Deformed Belt east of 72°W. Thus, Model 5 is a hybrid model that combines geological and geodetic data and results, taking into account slow slipping faults such as the Oca and the Caribbean Deformed Belt east of 72°W, whereas Model 4 takes into consideration only the faults that take up most of the relative motion between the Caribbean and the South American plates, that is, the faults that conform the main seismically active plate boundary between the two plates.

Taking into account both Models 4 and 5 in Fig. 10, the following observations are made: (1) Subduction rates along nearly north–south oriented segments of the Lesser Antilles subduction are 19.4–19.9 mm yr^{-1}, in agreement with the results reported by Symithe *et al.* (2015). The segments which depart from the north–south strike show a mechanically coherent strain partitioning that is dependent on segment's strike. (2) The easterly oriented El Pilar (P) fault in northeastern Venezuela and the plate boundary fault zone going across Trinidad (T) and then off-shore to the east both show a dextral slip of 19.3–19.8 mm yr^{-1}, in agreement with the geodetic results originally reported by Pérez *et al.* (2001), Weber *et al.* (2001, 2009), and also in agreement with the results provided by the kinematic block motion analysis of Symithe *et al.* (2015). (3) The northwest oriented Los Bajos–El Soldado (BS in Fig. 10) submarine fault system, located between Venezuela and Trinidad (T) shows dextral slip (13.7 mm yr^{-1}) and is transtensional (∼14 mm yr^{-1}), a type of motion early suggested by Pérez & Aggarwal (1981). (4) In both Models 4 and 5 in Fig. 10 the dextral relative plate motion in north–central Venezuela is partitioned between the San Sebastián (S, 17 mm yr^{-1}) and La Victoria (V, 2–2.3 mm yr^{-1}) faults, in agreement with the results of the elastic modelling we presented in an earlier section of the manuscript. (5) Taking into account both models, the Boconó (B) fault shows up to 10.2 mm yr^{-1} of dextral slip, and a component of convergence in the order of 2–6 mm yr^{-1}, in agreement with the results we derived in the previous section. (6) The Santa Marta (SM) fault shows a left-lateral slip rate of 1.2–2.0 mm yr^{-1}, and a convergence rate of 6.6–8.0 mm yr^{-1} depending on the model, in agreement with early GPS results reported by Trenkamp *et al.* (2002). (7) Subduction rate along the South Caribbean Marginal (SCM) fault segments ranges from ∼5 to ∼7 mm yr^{-1}. (8) Both models indicate that the Morrocoy (M) fault is right-lateral (2.9–4.8 mm yr^{-1}) and transtensional (∼4 mm yr^{-1}). (9) The existence of the Morrocoy boundary is compulsory to explain the observed velocity field in northwestern Venezuela and northern Colombia.

DISCUSSION AND CONCLUSIONS

The observed velocity field and corresponding modellings for the south–central Caribbean and north–central Venezuela regions, east of the triple junction vertex between the North Andes, Caribbean and South American plates (Figs 1, 2, 5 and 10) show that the ∼19.6 mm yr^{-1} of dextral relative motion of the Caribbean relative to South America is split with ∼17 mm yr^{-1} taken up by San Sebastián fault and ∼2.6 mm yr^{-1} by La Victoria fault. This latter rate of motion is highly consistent with geological estimates (∼2.75 mm yr^{-1}) of the Quaternary rate of motion of La Victoria fault zone (Audemard *et al.* 2000) near the epicentre of the 1641 earthquake (Fig. 2), where the fault is multibranched and is composed of several parallel strands. This partitioning of slip between subparallel faults is similar to the phenomenon occurring in the Hispaniola Island in northern Caribbean where the Caribbean–North America easterly left-lateral slip (18–20 mm yr^{-1}, DeMets *et al.* 2010) is divided among several eastward-trending faults that compose the plate boundary (Dixon *et al.* 1998; Calais *et al.* 2002; Symithe *et al.* 2015). And in some regards it is the same phenomenon taking place in the southern San Andreas fault system in California, where several subparallel faults accommodate plate motions (e.g. Lindsey & Fialko 2013).

The slip rate along San Sebastián fault is ∼5.5 times larger than the one along La Victoria fault and this may explain the much lower seismic moment productivity of the La Victoria fault compared to San Sebastián fault in the last ∼4 centuries (Pérez *et al.* 1997a) and qualifies the San Sebastián fault as the main strand of the plate boundary in the region. If slipping at ∼17 mm yr^{-1}, the ∼100 km long western segment of this fault (Fig. 2) has accumulated about 3.4 m of potential slip since it last broke in 1812 (Audemard 2002; Choy *et al.* 2010), sufficient to be released during a large strike-slip earthquake of $M_w > 7$, according to the scaling laws derived by Henry & Das (2001) and Wesnousky (2008).

Northwest of the North Andes–South American–Caribbean plates′ triple junction (Fig. 1) the Morrocoy fault zone marks the northeast boundary of the North Andes plate with the Caribbean plate (Pérez *et al.* 1997b; Bird 2003). Focal mechanisms along this fault system show northwest oriented dextral slip with a small component of normal faulting about 100 km northwest of the triple junction (Fig. 2), and normal faulting with a strike-slip component (Audemard *et al.* 2005) farther northwest around 12°N (Fig. 4). Right-lateral transtension is required across the Morrocoy fault because easterly directed GPS velocity vectors (Fig. 8) increase in magnitude and in azimuth as one moves from the North Andes plate to the Caribbean plate. As it was described in the previous section, from a kinematic block modelling we estimate the amount of dextral slip in ∼3–4.8 mm yr^{-1} along fault's strike and about 4 mm yr^{-1} of normal slip in the direction perpendicular to the fault. These observations are consistent with the observed focal mechanisms of seismic events straddling the Morrocoy fault (Figs 2 and 4) and also with geological and geophysical studies carried out in the region (Bellizzia *et al.* 1976; Beltrán 1993; Audemard *et al.* 2000; Gorney *et al.* 2007; Escalona & Mann 2011), which show the existence of active northwest striking Quaternary faults with normal and dextral slip both off-shore and inland. Fig. 11(a) is a map that compiles the known traces (coloured sinuous lines) of faults active since Tertiary in the regions adjacent to the Morrocoy (M) fault (Beltrán 1993; Audemard *et al.* 2000; Gorney *et al.* 2007; Escalona & Mann 2011; Castillo *et al.* 2017). Large portions of the Morrocoy boundary have not been seismically explored or the information is in the non-public oil industry domain. Fig. 11(b) shows a seismic reflection line collected during the BOLIVAR cruise in 2004 (Gorney *et al.* 2007; Escalona & Mann 2011) off-shore the Paraguaná Peninsula (PP, Fig. 11a). It shows normal faults cutting across the

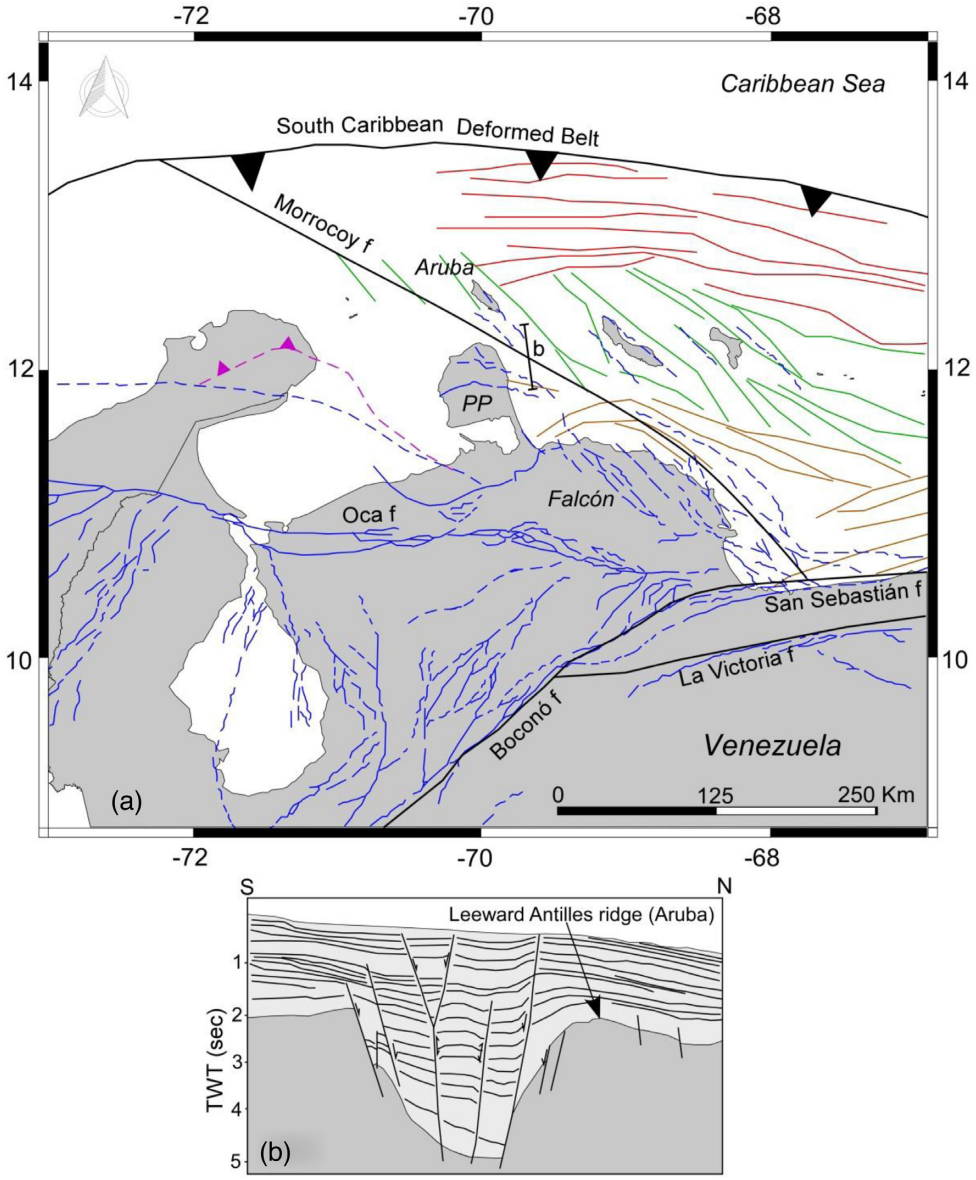

Figure 11. (a) Known Tertiary and younger faults (coloured sinuous lines) in western Venezuela and the Leeward Antilles, compiled from Beltrán 1993 (blue), Gorney *et al.* 2007 and Escalona & Mann 2011 (red, green and brown) and Castillo *et al.* 2017 (purple). PP, Paraguaná Peninsula. Main boundary faults are shown in black. (b) Seismic line located southeast of Aruba (Fig. 11a) with an interpreted graben structure (Gorney *et al.* 2007; Escalona & Mann 2011) that matches the proposed location of the Morrocoy fault.

basement in an area that matches the proposed location of the Morrocoy fault. Farther southeast the fault is apparently buried beneath a northwest trending thrust belt at the base of the Falcon slope.

In the most northwestern regions of the South American continent, using teleseismic and microseismicity data we have improved the knowledge of the geometry concerning the northeast striking, southeast dipping subduction of the Caribbean plate beneath the North Andes plate (Figs 6–8), and have shown this subduction is oblique to the Caribbean–South America slip vector. Also, the modelled rate of southeast subduction of the Caribbean plate relative to the North Andes plate (Fig. 10) is rather small (5–7 mm yr^{-1}), which explains the low background seismic activity in the region. Indeed, the Benioff zone in northwestern Venezuela is better defined only when microearthquake locations are considered. This small relative rate of subduction implies that 2000–3000 yr of strain accumulation are needed for a potential giant ($M_w > 8.5$) shock with a co-seismic slip of up to 15 m or more to break the entire 500–600 km long interplate boundary, a rupture length typical for events of this size (e.g. Thatcher 1990; Pérez & Scholz 1997), as it was the case during the 2010 M_w 8.8 Chilean earthquake (e.g. Vigny *et al.* 2011; Wang *et al.* 2012). At this time scale the seismic history of the region is completely unknown. A smaller yet strong event would need a smaller strain accumulation time. For instance, it would take around 300–600 yr to accumulate 2–3 m of slip, equivalent to the average slip that would be expected in an M_w 7.5–7.8 subduction earthquake with a rupture length on the order of 130 km (e.g. Henry & Das 2001; Wesnousky 2008).

Southwest of the triple junction the interaction between the North Andes and South American plates along the Boconó fault zone and Venezuelan Andes occurs in such a way that slip partitioning takes place with 9–11 mm yr^{-1} of dextral motion in the far field of the fault and 2–5 mm yr^{-1} of shortening across the Venezuelan Andes.

Thus, the slip partitioning exhibited by this region resembles that occurring in Central California where thrust faulting occurs on planes that strike near parallel to the San Andreas fault, as in the 1983 Coalinga shock and related events (Stein & King 1984; Ekström & England 1989; Stein & Ekström 1992). As along the central San Andreas fault, focal mechanisms reported for the area (e.g. Pérez *et al.* 1997b) show pure dextral motion for microseisms associated with the Boconó fault itself, whereas many microearthquakes located well away from the fault and along the Andean foothills show pure thrust motion on planes dipping towards the Boconó fault.

Several authors have proposed (e.g. Kellogg & Bonini 1982, 1985; Kellogg *et al.* 1985; Kellogg & Vega 1995; Trenkamp *et al.* 2002) that dextral motion along the Oriente, East Andean and Boconó faults in Ecuador, Colombia and Venezuela, respectively (Fig. 1), is accommodating the northward component of motion of the North Andes plate that results from a squeezing of the plate between the Nazca plate and the Oriente and East Andean faults. While this idea is acceptable and is consistent with our GPS data, the transtensional right-lateral motion we observe along the Morrocoy fault requires that the resulting eastward component of North Andean motion remains less than that of the Caribbean plate. Finally, the GPS coverage for the southern Caribbean region is being significantly improved thanks to the implementation by UNAVCO of a wide aperture GPS array, the COCOnet GPS network, covering the whole Caribbean and adjacent regions. Thus, it is expected that refinements in the knowledge of the kinematics of the region and subsequent quantification of seismic hazards will arise as new observations are collected.

ACKNOWLEDGEMENTS

New GPS observations in Venezuela were funded by Simón Bolívar University. We thank the Colombian Geological Survey for providing seismic data and a series of GPS velocity vectors of sites in Colombian territory. David Mencin provided us with several unpublished velocity vectors and helped us in the geodetic data processing. UNAVCO provided data from sites that belong to the COCOnet GPS array. We are grateful to John P. Loveless for his help to use the software 'Blocks'. Our former students Yuleika Madriz, Freddy Rondón, Carlos Moncayo, Mizael Bravo and the Physical and Satellite Geodesy Laboratory of La Universidad del Zulia in Maracaibo, Venezuela, took care of the new data gathering. Comments and suggestions made by Editor Juan C. Afonso, Eric Calais and by an anonymous reviewer led to a significant improvement of our work. Roger Bilham provided us with GPS data he collected in Aruba in 2012. In memoriam of LL who passed away during the preparation of the manuscript.

REFERENCES

Altamimi, Z., Collileux, X. & Métivier, I., 2011. ITRF2008: an improved solution of the international terrestrial reference frame, *J. Geod.,* **85,** 45–473.

Altamimi, Z., Metivier, L. & Collilieux, X., 2012. ITRF2008 plate motion model, *J. geophys. Res.,* **117,** B07402, doi:10.1029/2011JB008930.

Altez, R., 1998. Cronometrización extemporánea: Los sismos del 26 de Marzo de 1812 en Caracas y en Mérida, *Rev. Geog. Vla.,* **39,** 297–326.

Audemard, F.A., 1996. Paleoseismicity studies on the Oca-Ancon fault system, northwestern Venezuela, *Tectonophysics,* **259,** 67–80.

Audemard, F.A., 2002. Ruptura de los grandes sismos históricos venezolanos de los siglos XIX y XX revelados por la sismicidad instrumental contemporánea, in *XI Congreso Venezolano de Geofísica,* Caracas, Venezuela, pp. 8, 17–20 Noviembre, CD format.

Audemard, F.A., Machette, M., Cox, J., Dart, R. & Haller, K., 2000, Map at scale 1:2.000.000 and database of Quaternary Faults in Venezuela and its offshore regions, Open-File Rep 00–0018, U.S. Geol. Surv., pp. 78.

Audemard, F.A., Romero, G., Rendón, H. & Cano, V., 2005. Quaternary fault kinematics and stress tensor along the southern Caribbean from fault-slip data and focal mechanism solutions, *Earth-Sci. Rev.,* **69,** 181–233.

Audemard, F.E. & Audemard, F.A., 2002. Structure of the Mérida Andes, Venezuela: relations with the South America–Caribbean geodynamic interaction, *Tectonophysics,* **345,** 299–327.

Bellizzia, A., Pimentel, N. & Bajo, R., 1976. *Structural Geology Map of Venezuela, Scale: 1: 500.000,* Min. Minas e Hidrocarburos.

Beltrán, C., 1993. *Mapa Neotectónico de Venezuela, esc: 1:2.000.000,* Fundación Venezolana de Investigaciones Sismológicas (FUNVISIS).

Bernal-Olaya, R., Mann, P. & Vargas, C.A., 2015. Earthquake, tomographic, seismic reflection, and gravity evidence for a shallowly dipping subduction zone beneath the Caribbean Margin of northwestern Colombia, in *Petroleum Geology and Potential of the Colombian Caribbean Margin,* Vol. 108, pp. 247–270, eds Bartolini, C. & Mann, P., AAPG Memoir.

Bird, P., 2003. An updated digital model of plate boundaries, *Geochem. Geophys. Geosys.,* **4,** doi:10.1029/2001GC000252.

Calais, E., Mazabraud, Y., de Lépinay, B.M., Mann, P., Mattioli, G. & Jansma, P, 2002. Strain partitioning and fault slip rates in the northeastern Caribbean from GPS measurements, *Geophys. Res. Lett.,* **29,** 3–1-3-4.

Camacho, E., Hutton, W. & Pacheco, J.F., 2010. A new look at evidence for a Wadati-Benioff Zone and active convergence at the north Panama deformed belt, *Bull. seism. Soc. Am.,* **100,** 343–348.

Castillo, V., Benkovics, L., Cobos, C., Demuro, D. & Franco, A., 2017. Perla field: the largest discovery ever in Latin America, in *Giant Fields of the Decade 2000–2010,* Vol. 113, pp. 141–152, eds Merrill, R.K. & Sternbach, C.A., AAPG Memoir.

Centeno-Graű, M., 1900. El Terremoto de 1900, in *La Linterna Mágica*.

in 1900. The reference is given as is by other authorsCenteno-Graű, M., 1940. *Estudios Sismológicos,* 300 pp., Litografía del Comercio.

Chiarabba, C., De Gori, P., Faccenna, C., Speranza, F., Seccia, D., Dionicio, V. & Prieto, G.A., 2015. Subduction system and flat slab beneath the Eastern Cordillera of Colombia, *Geochem. Geophys. Geosyst.,* **17,** 16–27.

Choy, J.E., 2001. The El Tocuyo, Venezuela, earthquake of 3 August, 1950: focal parameters and tectonic implications, *Geofís. Int.,* **40,** 285–292.

Choy, J.E., Palme, C., Guada, C., Morandi, M. & Klarica, S., 2010. Macroseismic Interpretation of the 1812 earthquake in Venezuela using intensity uncertainties and *a priori* fault-strike information, *Bull. seism. Soc. Am.,* **100,** 241–255.

Clark, S.A., Zelt, C.A., Magnani, M.B. & Levander, A., 2008. Characterizing the Caribbean–South American plate boundary at 64° west using wide-angle seismic data, *J. geophys. Res,* **113,** B07401,.

Colombian Geological Survey, 2016. 'Earthquake locations, National Seismological Array '. Available at: www.sgc.gov.co/.

Colón, S. *et al.*, 2015. The 1900 M_w 7.6 earthquake offshore north–central Venezuela: is La Tortuga or San Sebastián the source fault? *Mar. Pet. Geol.,* **67,** 498–511.

Dach, R., Hugentobler, U., Fridez, P. & Meindl, M., 2007. *Bernese GPS Software Version 5.0,* University of Bern, Bern Open Publishing,.

DANE, 2016. 'Departamento Administrativo Nacional de Estadísticas de Colombia', Available at: http://www.dane.gov.co/.

DeMets, C., Gordon, R.G., Argus, F. & Stein, S., 1990. Current plate motions, *Geophys. J. Int.,* **101,** 425–478.

DeMets, C., Gordon, R.G. & Argus, D.F., 2010. Geologically current plate motions, *Geophys. J. Int.,* **181,** 1–80.

Dewey, J.W., 1972. Seismicity and tectonics of western Venezuela, *Bull. seism. Soc. Am.,* **62,** 1711–1751.

Dixon, T.H., Farina, F., DeMets, C., Jansma, P., Mann, P. & Calais, E., 1998. Relative motion between the Caribbean and North American plates and related boundary zone of deformation from a decade of GPS observations, *J. geophys. Res.,* **103,** 15 157–15 182.

Ekström, G. & England, P.C., 1989. Seismic strain rates in regions of distributed continental deformation, *J. geophys. Res.,* **94,** 10 231–10 257.

Ernst, A., 1878. Eartquake in Venezuela, *Nature,* **18,**.

Escalona, A. & Mann, P., 2011. Tectonics, basin subsidence mechanisms, and paleogeography of the Caribbean-South American plate boundary zone, *Mar. Pet. Geol.,* **28,** 8–39.

Fielder, G., 1961. Areas afectadas por terremotos en Venezuela, *Venez. Geol. Conf. Bol. Geol.,* **4,** 1791–1810.

FUNVISIS, 2016. 'Venezuelan Foundation for Seismological Research, Earthquake Catalogs', Available at: http://www.funvisis.gob.ve/.

Grases, J., 1980, Investigación sobre los sismos destructores que han afectado el occidente y centro-norte de Venezuela, Tech. Rep., INTEVEP, p. 301.

Gorney, D., Escalona, A., Mann, P. & Magnani, M.B., BOLIVAR Study Group, 2007. Chronology of Cenozoic tectonic events in western Venezuela and the Leeward Antilles based on integration of offshore seismic reflexion and on-land geology, *AAPG Bull*., **91,** 653–684.

Guzmán, O. *et al.*, 2013. ^{10}Be dating of river terraces of Santo Domingo river, on Southeastern flank flank of the Mérida Andes, Venezuela: tectonic and climatic implications, *J. South Am. Earth Sci.,* **48,** 85–96.

Henry, C. & Das, S., 2001. Aftershocks of large shallow earthquakes: fault dimensions, aftershock area expansion and scaling relations, *Geophys. J. Int.,* **147,** 272–293.

Idárraga-García, J. & Romero, J., 2010. Neotectonic study of the Santa Marta Fault System, western foothills of the Sierra Nevada de Santa Marta, Colombia, *J. South Am. Earth Sci.,* **29,** 849–860.

Instituto Nacional de Estadísticas (INE), 2011. 'XIV Censo Nacional de Población y Vivienda', Available at: http://www.ine.gov.ve/.

ISC, 2013. 'International Seismological Centre, on-line bulletin ', Availabl e at: http://www.isc.ac.uk.

Jordan, T.H., 1975. The present-day motion of the Caribbean plate, *J. geophys. Res.,* **80,** 4433–4440.

Jouanne, F., Audemard, F., Beck, C., Van Welden, A., Ollarves, R. & Reinoza, C., 2011. Present-day deformation along the El Pilar Fault in eastern Venezuela: evidence of creep along a major transform boundary, *J. Geodyn.,* **51,** 398–410.

Kellogg, J.N., 1984. Cenozoic tectonic history of the Sierra de Perijá, Venezuela-Colombia, and adjacent basins, *Geol. Soc. Am. Mem.,* **162,** 239–261.

Kellogg, J.N. & Bonini, W.E., 1982. Subduction of the Caribbean plate and basement uplifts in the overriding South American plate, *Tectonics,* **1,** 251–276.

Kellogg, J.N. & Bonini, W.E., 1985. Reply to comment on "Subduction of the Caribbean plate and basement uplifts in the overriding South American plate", by C. Schubert, *Tectonics,* **4,** 785–790.

Kellogg, J.N. & Vega, V., 1995. Tectonic development of Panamá, Costa Rica, and the Colombian Andes: constraints from Global Positioning System geodetic studies and gravity, *Geol. Soc. Am. Spec. Pap.,* **295,** 75–90.

Kellogg, J.N., Ogujiofor, I.J. & Kansaka, D.R., 1985. Cenozoic tectonics of the Panamá and North Andes block, in *Memorias VI Congreso Latino-Americano de Geología,* pp. 34–49.

Kroehler, M.E., Mann, P., Escalona, A. & Christeson, G.L., 2011. Late Cretaceous-Miocene diachronous onset of back thrusting along the South Caribbean deformed belt and its importance for understanding processes of arc collision and crustal growth, *Tectonics,* **30,** TC6003,.

Lindsey, E.O. & Fialko, Y., 2013. Geodetic slip rates in the southern San Andreas Fault system: effects of elastic heterogeneity and fault geometry, *J. geophys. Res.,* **118,** 689–697.

Loveless, J.P. & Meade, B.J., 2010. Geodetic imaging of plate motions, slip rates, and partitioning of deformation in Japan, *J. geophys. Res.,* **115,**.

Magnani, M.B., Zelt, C.A., Levander, A. & Schmitz, M., 2009. Crustal structure of the South American–Caribbean plate boundary at 67°W from controlled source seismic data, *J. geophys. Res.,* **114,** B02312,.

Malavé, G. & Suárez, G., 1995. Intermediate depth seismicity in northern Colombia and western Venezuela and its relationship to Caribbean plate subduction, *Tectonophysics,* **14,** 617–628.

Manaker, D.M. *et al. et al*, 2008. Interseismic plate coupling and strain partitioning in the northeastern Caribbean, *Geophys. J. Int.,* **174,** 889–903.

McCaffrey, R., 2002. Crustal block rotations and plate coupling, in *Plate Boundary Zones,* pp. 101–122, eds Stein, S. & Freymueller, J., American Geophysical Union.

Meade, B.J. *et al.*, 2002. Estimates of seismic potential in the Marmara Sea region from block models of secular deformation constrained by Global Positioning System measurements, *Bull. seism. Soc. Am.,* **92,** 208–215.

Meade, B.J & Loveless, J.P., 2009. Block modeling with connected fault-network geometries and a linear elastic coupling estimator in spherical coordinates, *Bull. seism. Soc. Am.,* **99,** 3124–3139.

McKenzie, D.P. & Morgan, W.J., 1969. Evolution of triple junctions, *Nature,* **224,** 125–133.

Mora-Páez, H., Giraldo-Londoño, L., Cardona-Piedrahita, L., Peláez-Gaviria, J. & Lizarazo, S., 2016a. Velocidades geodésicas horizontales de Colombia, Grupo de Investigaciones Geodésicas Espaciales, Proyecto GeoRED, Servicio Geológico Colombiano, Documento Interno, Bogotá.

Mora-Páez, H., Mencin, D.J., Molnar, P., Diederix, H., Cardona-Piedrahita, L., Peláez-Gaviria, J-R. & Corchuelo-Cuervo, Y., 2016b. GPS velocities and the construction of the Eastern Cordillera of the Colombian Andes, *Geophys. Res. Lett.,* **43,** 8407–8416.

Okada, Y., 1985. Surface deformation due to shear and tensile faults in a half-space, *Bull. seism. Soc. Am.,***75,** 1135–1154.

Pacheco, J.F. & Sykes, L.R., 1992. Seismic moment catalog of large shallow earthquakes, 1900 to 1989, *Bull. seism. Soc. Am.,* **82,** 1306–1349.

Paris, G., Machette, M.N., Dart, R.L. & Haller, K.M., 2000, Map and Database of Quaternary Faults and Folds in Colombia and its Offshore Regions, Open-File Rep 00–0284, U.S. Geol. Surv., pp. 61.

Pennington, W.D., 1981. Subduction of the eastern Panamá basin and seismotectonics of northwestern South America, *J. geophys. Res.,* **80,** 10 753–10 770.

Pérez, O.J. *et al.*, 2001. Velocity field across the southern Caribbean plate boundary and estimates of Caribbean/South American plate motion using GPS geodesy 1994–2000, *Geophys. Res. Lett.,* **28,** 2987–2990.

Pérez, O.J. *et al.*, 2011. Campo de velocidades en el occidente de Venezuela: componente lateral derecha asociada a la falla de Boconó y componente convergente perpendicular a los Andes, *Interciencia,* **36,** 39–44.

Pérez, O.J. & Aggarwal, Y.P., 1981. Present-day tectonics of the southern Caribbean and northeastern Venezuela, *J. geophys. Res.,* **86,** 791–804.

Pérez, O.J. & Mendoza, J.S., 1998. Sismicidad y tectónica en Venezuela y áreas vecinas, *Fís. Tierra,* **10,** 87–110.

Pérez, O.J. & Scholz, C.H., 1997. Long-term seismic behavior of the focal and adjacent regions of great earthquakes during the time between two successive shocks, *J. geophys. Res.,* **102,** 8203–8216.

Pérez, O.J., Jaimes, M. & Garciacaro, E., 1997b. Microseismicity evidence for subduction of the Caribbean plate beneath the South American plate in northwestern Venezuela, *J. geophys. Res.,* **102,** 17 875–17 882.

Pérez, O.J., Sanz, C. & Lagos, G., 1997a. Microseismicity, tectonics and seismic potential in southern Caribbean and northern Venezuela, *J. Seismol.,* **1,** 15–28.

Reilinger, R. *et al.*, 2006. GPS constraints on continental deformation in the Africa-Arabia-Eurasia continental collision zone and implications for the dynamics of plate interactions, *J. geophys. Res.,* **111,** doi:10.1029/2005JB004051.

Reinoza, C., Jouanne, F., Audemard, F.A., Schmitz, M. & Beck, C., 2015. Geodetic exploration of strain along the El Pilar fault in northeastern Venezuela, *J geophys. Res.,* **120,** 1993–2013.

Rial, J.A., 1978. The Caracas, Venezuela, earthquake of July 1967: a multiple source event, *J. geophys. Res.,* **83,** 5405–5414.

Saria, E., Calais, E., Stamps, D., Delvaux, D. & Hartnady, C., 2014. Present-day kinematics of the East African rift, *J. geophys. Res.,* **119,** 3584–3600.

Schmitz, M. *et al.*, 2008, Crustal thickness variations in Venezuela from deep seismic observations, *Tectonophysics,* **459,** 14–26.

Sievers, W., 1905. Das Erdbeben in Venezuela von 29 Oktober 1900, Fest zur Feier des 70 Geburtstages von J. J. Rein, Jahrb Veroffnet. Geog. Verein. zu Bonn, 35–50.

Silver, E.A., Case, J.E. & MacGillvary, H.J., 1975. Geophysical study of the Venezuelan borderland, *Bull. geol. Soc. Am.,* **86,** 213–226.

Symithe, S., Calais, E., de Chabalier, J.B., Robertson, R. & Higgins, M., 2015. Current block motions and strain accumulation on active faults in the Caribbean, *J. geophys. Res.,* **120,** 3748–3774.

Syracuse, E.M., Maceira, M., Prieto, G.A., Zhang, H. & Ammon, C.J., 2016. Multiple plates subducting beneath Colombia, as illuminated by seismicity and velocity from the joint inversion of seismic and gravity data, *Earth planet. Sci. Lett.,* **444,** 139–149.

Stein, R. & King, G., 1984. Seismic potencial revealed by surface folding: 1993 Coalinga, California earthquake, *Science,* **224,** 869–872.

Stein, R.S. & Ekström, G., 1992. Seismicity and geometry of a 110-km-long blind thrust fault 2. Synthesis of the 1982–1985 earthquake sequence, *J. geophys. Res.,* **97,** 4865–4884.

Talwani, M., Windish, C.C., Stoffa, P.L., Buhl, P. & Houtz, R.E., 1977. Multichannel seismic study of the Venezuelan basin and the Curaçao ridge, in *Island Arcs, Deep Sea Trenches and Back-Arc Basins, Maurice Ewing Series,* pp. 83–98, eds Talwani, M. & Pitman, W.C., III, American Geophysical Union.

Thatcher, W., 1990. Order and diversity in the modes of Circum-Pacific earthquake occurrence, *J. geophys. Res.,* **95,** 2609–2623.

Toto, E.A. & Kellogg, J.N., 1992. Structure of the Sinu-San Jacinto fold belt—an active accretionary prism in northern Colombia, *J. South Am. Earth Sci.,* **5,** 211–222.

Trenkamp, R., Kellogg, J.N., Freymueller, J.T. & Mora, H.P., 2002. Wide plate margin deformation, southern Central America and northwestern South America, CASA GPS observations, *J. South Am. Earth Sci.,* **15,** 157–171.

van der Hilst, R & Mann, P., 1994. Tectonic implications of tomographic images of subducted lithosphere beneath northwestern South America, *Geology,* **22,** 451–454.

Vigny, C. *et al.*, 2011. The 2010 M_w 8.8 Maule megathrust earthquake of Central Chile, monitored by GPS, *Science,* **332,** 1417–1421.

Wang, L. *et al.*, 2012. Coseismic slip of the 2010 M_w 8.8 Great Maule, Chile, earthquake quantified by the inversion of GRACE observations, *Earth planet. Sci. Lett.,* **335–336,** 167–179.

Weber, J. *et al.*, 2001. GPS estimate of relative motion between the Caribbean and South American plates, and geological implications for Trinidad and Venezuela, *Geology,* **29,** 75–78.

Weber, J.C., Saleh, J., Balkaransingh, S., Dixon, T., Ambeh, W., Leong, T., Rodriguez, A. & Miller, K., 2009. Triangulation-to-GPS and GPS-to-GPS geodesy in Trinidad, West Indies: neotectonics, seismic risk, and geologic implications, *Mar. Pet. Geol.,* **28,** 200–211.

Wesnousky, S.G., 2008. Displacement and geometrical characteristics of earthquake surface ruptures: issues and implications for seismic-hazard analysis and the process of earthquake rupture, *Bull. seism. Soc. Am.,* **98,** 1609–1632.

Wesnousky, S.G., Araguren, R., Rengifo, M., Owen, L.A., Caffee, M.W., Murari, M.K. & Pérez, O.J., 2012. Toward quantifying geomorphic rates of crustal displacements, landscape development, and the age of glaciation in the Venezuelan Andes, *Geomorphology,* **141–142,** 99–113.

Key words

Authors are requested to choose key words from the list below to describe their work. The key words will be printed underneath the summary and are useful for readers and researchers. Key words should be separated by a semi-colon and listed in the order that they appear in this list. An article should contain no more than six key words.

COMPOSITION and PHYSICAL PROPERTIES
Composition and structure of the continental crust
Composition and structure of the core
Composition and structure of the mantle
Composition and structure of the oceanic crust
Composition of the planets
Creep and deformation
Defects
Elasticity and anelasticity
Electrical properties
Equations of state
Fault zone rheology
Fracture and flow
Friction
High-pressure behaviour
Magnetic properties
Microstructure
Permeability and porosity
Phase transitions
Plasticity, diffusion, and creep

GENERAL SUBJECTS
Core
Gas and hydrate systems
Geomechanics
Geomorphology
Glaciology
Heat flow
Hydrogeophysics
Hydrology
Hydrothermal systems
Instrumental noise
Ionosphere/atmosphere interactions
Ionosphere/magnetosphere interactions
Mantle processes
Ocean drilling
Structure of the Earth
Thermochronology
Tsunamis
Ultra-high pressure metamorphism
Ultra-high temperature metamorphism

GEODESY and GRAVITY
Acoustic-gravity waves
Earth rotation variations
Geodetic instrumentation
Geopotential theory
Global change from geodesy
Gravity anomalies and Earth structure
Loading of the Earth
Lunar and planetary geodesy and gravity
Plate motions
Radar interferometry
Reference systems
Satellite geodesy
Satellite gravity
Sea level change
Seismic cycle
Space geodetic surveys
Tides and planetary waves
Time variable gravity
Transient deformation

GEOGRAPHIC LOCATION
Africa
Antarctica
Arctic region
Asia
Atlantic Ocean
Australia
Europe
Indian Ocean
Japan
New Zealand
North America
Pacific Ocean
South America

GEOMAGNETISM and ELECTROMAGNETISM
Archaeomagnetism
Biogenic magnetic minerals
Controlled source electromagnetics (CSEM)
Dynamo: theories and simulations
Electrical anisotropy
Electrical resistivity tomography (ERT)
Electromagnetic theory
Environmental magnetism
Geomagnetic excursions
Geomagnetic induction
Ground penetrating radar
Magnetic anomalies: modelling and interpretation
Magnetic fabrics and anisotropy
Magnetic field variations through time
Magnetic mineralogy and petrology
Magnetostratigraphy
Magnetotellurics
Marine electromagnetics
Marine magnetics and palaeomagnetics
Non-linear electromagnetics
Palaeointensity
Palaeomagnetic secular variation
Palaeomagnetism
Rapid time variations
Remagnetization
Reversals: process, time scale, magnetostratigraphy
Rock and mineral magnetism
Satellite magnetics

GEOPHYSICAL METHODS
Downhole methods
Fourier analysis
Fractals and multifractals
Image processing
Instability analysis
Interferometry
Inverse theory
Joint inversion
Neural networks, fuzzy logic
Non-linear differential equations
Numerical approximations and analysis
Numerical modelling
Numerical solutions
Persistence, memory, correlations, clustering
Probabilistic forecasting
Probability distributions
Self-organization
Spatial analysis
Statistical methods
Thermobarometry
Time-series analysis
Tomography
Waveform inversion
Wavelet transform

PLANETS
Planetary interiors
Planetary volcanism

SEISMOLOGY
Acoustic properties
Body waves
Coda waves
Computational seismology
Controlled source seismology
Crustal imaging
Earthquake dynamics
Earthquake early warning
Earthquake ground motions
Earthquake hazards
Earthquake interaction, forecasting, and prediction
Earthquake monitoring and test-ban treaty verification
Earthquake source observations
Guided waves
Induced seismicity
Interface waves
Palaeoseismology
Rheology and friction of fault zones
Rotational seismology
Seismic anisotropy
Seismic attenuation
Seismic instruments
Seismic interferometry
Seismicity and tectonics
Seismic noise
Seismic tomography
Site effects
Statistical seismology
Surface waves and free oscillations
Theoretical seismology
Tsunami warning

Volcano seismology
Wave propagation
Wave scattering and diffraction

TECTONOPHYSICS
Backarc basin processes
Continental margins: convergent
Continental margins: divergent
Continental margins: transform
Continental neotectonics
Continental tectonics: compressional
Continental tectonics: extensional
Continental tectonics: strike-slip and transform
Cratons
Crustal structure
Diapirism
Dynamics: convection currents, and mantle plumes
Dynamics: gravity and tectonics
Dynamics: seismotectonics
Dynamics and mechanics of faulting
Dynamics of lithosphere and mantle
Folds and folding
Fractures, faults, and high strain deformation zones
Heat generation and transport
Hotspots
Impact phenomena
Intra-plate processes
Kinematics of crustal and mantle deformation
Large igneous provinces
Lithospheric flexure
Mechanics, theory, and modelling
Microstructures
Mid-ocean ridge processes
Neotectonics
Obduction tectonics
Oceanic hotspots and intraplate volcanism
Oceanic plateaus and microcontinents
Oceanic transform and fracture zone processes
Paleoseismology
Planetary tectonics
Rheology: crust and lithosphere
Rheology: mantle
Rheology and friction of fault zones
Sedimentary basin processes
Subduction zone processes
Submarine landslides
Submarine tectonics and volcanism
Tectonics and climatic interactions
Tectonics and landscape evolution
Transform faults
Volcanic arc processes

VOLCANOLOGY
Atmospheric effects (volcano)
Calderas
Effusive volcanism
Eruption mechanisms and flow emplacement
Experimental volcanism
Explosive volcanism
Lava rheology and morphology
Magma chamber processes
Magma genesis and partial melting
Magma migration and fragmentation
Mud volcanism
Physics and chemistry of magma bodies
Physics of magma and magma bodies
Planetary volcanism
Pluton emplacement
Remote sensing of volcanoes
Subaqueous volcanism
Tephrochronology
Volcanic gases
Volcanic hazards and risks
Volcaniclastic deposits
Volcano/climate interactions
Volcano monitoring
Volcano seismology